Assessment of a Monumental Masonry Bell-Tower After 2016 Central Italy Seismic Sequence by Long-term SHM

Filippo Ubertini, Nicola Cavalagli, Alban Kita and Gabriele Comanducci

University of Perugia, Department of Civil and Environmental Engineering, Via G. Duranti 93, Perugia, Italy

Tel.: +39-075-5853954

Fax: +39-075-5853830

filippo.ubertini@unipg.it (Filippo Ubertini)

Abstract. The response of the San Pietro monumental bell-tower located in Perugia, Italy, to the 2016 Central Italy seismic sequence is investigated, taking advantage of the availability of field data recorded by a vibration-based SHM system installed in December 2014 to detect earthquake-induced damages. The tower is located about 85 km in the NW direction from the epicenter of the first major shock of the sequence, the Accumoli Mw6.0 earthquake of August 24th, resulting in a small local PGA of about 30 cm/s^2, whereby near-field PGA was measured as 915.97 cm/s^2 (E-W component) and 445.59 cm/s^2 (N-S component). Similar PGA values also characterized the two other major shocks of the sequence (Ussita Mw5.9 and Norcia Mw6.5 earthquakes of October 26th and 30th, respectively). Despite the relatively low intensity of such earthquakes in Perugia, the analysis of long-term monitoring data clearly highlights that small permanent changes in the structural behavior of the bell-tower have occurred after the earthquakes, with decreases in all identified natural frequencies. Such natural frequency decays are fully consistent with what predicted by non-linear finite element simulations and, in particular, with the development of microcracks at the base of the columns of the belfry. Microcracks in these regions, and in the rest of tower, are however hardly distinguishable from pre-existing ones and from the physiological cracking of a masonry structure, what validates the effectiveness of the SHM system in detecting earthquake-induced damage at a stage where this is not yet detectable by visual inspections.

Keywords. Earthquake-induced damage detection; Structural health monitoring; Structural assessment; Heritage structures; Preventive conservation.

1. Introduction

Structural health monitoring (SHM) systems are aimed at the automated assessment of structural performance and at tracking its evolution in time, using data acquired by sensing systems (Deraemaeker et al, 2008; Kaya and Safak, 2015). Among the different available approaches for SHM, long-term vibration-based systems are receiving an increasing attention, including notable applications for post-earthquake structural assessment (Spina et al, 2011; Bindi et al, 2016; Pitilakis et al, 2016; Dolce et al, 2017). Such systems are typically based on a continuous acquisition of the dynamic response of a structure in operational conditions and in the application of suitable statistical tools to extract damage sensitive features from the data, removing the effects of changing environmental conditions and revealing, in an automated way, the formation of a small damage in the structure. Most of the currently available approaches are based on the continuous modal identification of the structure (Magalhes et al, 2009; Rainieri and Fabbrocino, 2010; Reynders et al, 2012; Ubertini et al, 2013) and in the inspection of anomalies in the time series of the natural frequencies of vibration using unsupervised learning techniques (Fugate et al, 2001; Sohn et al, 2002; Oh and Sohn, 2009; Farrar and Worden, 2012). In similar approaches, an initial period necessary to build and train the statistical models is required to fully characterize the normal conditions. Since temperature is the main environmental driver of changes in natural frequencies of structures, the full characterization of the normal conditions typically requires one year of training, which is necessary to observe long-term seasonal variations of environmental conditions. When sufficient training data have been collected, the SHM becomes effective.

Literature counts several applications of ambient vibration testing and Operational Modal Analysis (OMA), including infrastructural systems (Gentile and Gallino, 2008; Magalhes et al, 2009) and heritage structures (Peeters and De Roeck, 2001; Jaishi et al, 2003; Bennati et al, 2005; Ivorra and Pallars, 2006; Gentile and Saisi, 2007; Brencich and Sabia, 2008; Ramos et al, 2010; Aras et al, 2011; Ramos et al, 2011; Foti et al, 2012; Cury and Cremona, 2012; Gentile and Saisi, 2013; Cross et al, 2013; Dervilis et al, 2014; Gentile et al, 2015). In recent years, the improvement in OMA techniques has led to the application of long-term output-only vibration-based SHM in the same contexts (Ntotsios et al, 2008; Magalhes et al, 2012; Comanducci et al, 2015; Saisi et al, 2015; Comanducci et al, 2016; Ubertini et al, 2016b, 2017). Overall, however, practical demonstrations of the ability of vibration-based SHM systems to actually detect a small damage that could not be detected by a mere visual inspection are still missing.

Among the tools available for long-term vibration-based SHM, one has to discriminate between those useful for removing environmental effects from identified natural frequencies (also referred to as data cleansing procedures) and those useful for detecting deviations from normal conditions in the cleansed data. Principal Component Analysis (PCA) is a well-known technique that can address the first task when statistical correlations between natural frequencies and environmental parameters are linear (Yan et al, 2005a; Bellino et al, 2010). The main advantage of PCA is that it does not require to measure the environmental conditions. Several improvements to classic PCA have been proposed in the literature to handle the more general case of non-linear correlations between damage-sensitive features, such as Kernel PCA and local PCA (Kambhatla and Leen, 1997; Yan et al, 2005b). When environmental conditions, such as temperature and humidity, are measured, statistical models can be built linking such quantities, treated as statistical predictors, to natural frequencies. This is for instance the case when using input-output models such as autoregressive models (Bodeux and Golinval, 2001; Yong and Feng, 2005), multiple linear regressions (Dervilis et al, 2015), neural networks and so forth. More recently, cointegration has also been proposed as a tool to identify non stationary properties in time series of monitoring data for SHM purposes (Cross et al, 2011; Cross and Worden, 2012). The task of detecting deviations from normal conditions is typically carried out by statistical process control tools, namely by control charts based on proper statistical distances, such as Q^2 and T^2 statistics (Worden et al, 2000; Sohn et al, 2002;Worden et al, 2002; Fuller, 2009; Mosavi et al, 2012).

The application of long-term SHM systems is especially promising in the field of earthquake engineering (Ponzo et al, 2010; Farrar and Beck, 2015; Goulet et al, 2015), where ambient vibration testing and operational modal analysis have been profitably applied in recent years (Casarin and Modena, 2008; Pea et al, 2010; Ditommaso et al, 2012; Vidal et al, 2014; Benedettini et al, 2017). These systems allow to (i) highlight if a structure has undergone permanent damage after a shock or if it is accumulating damage during an earthquake sequence, (ii) to check if a damaging process is stable in time or it tends to get worse and (iii) to compare the response of different monitored structures after an event, so as to optimize and prioritize the control activities and the restoration interventions.

This paper presents an analysis of the response of the San Pietro monumental bell-tower located in Perugia, Italy, to the Accumoli earthquake of August 24th 2016 and to the two following major shocks of the same seismic sequence and, in particular, Ussita earthquake of October 26th 2016 and Norcia earthquake of October 30th 2016. The study of the response of this structure represents a notable scientific opportunity to practically evaluate the potential of vibration-based SHM systems in a general framework of preventive conservation of monumental structures exposed to the seismic hazard. The bell-tower has been monitored by the authors for more than two years, using high sensitivity accelerometers deployed on top of the tower and processing data with a technique based on (i) an automated modal identification tool based on data-driven Stochastic Subspace Identification (SSI), (ii) PCA applied to time series of identified natural frequencies to remove the effects of changing environmental conditions and (iii) control charts. As shown in the paper, although the structure is located far from the epicenters of the earthquakes, which resulted in small values of input PGA, permanent changes in its dynamic behavior are clearly highlighted after each shock of the seismic sequence. A non-linear dynamic analysis using a calibrated finite element model of the structure highlights a very good match between predicted and measured structural responses and also reveals that, during the earthquakes, some parts of the structure, notably the bases of the columns of the belfry, accumulated irreversible damage under tensile stress. A linear modal analysis carried out on the damaged model finally shows that the effects of such a damage on the natural frequencies are fully consistent with the decays observed from field data and with the deviations highlighted by the control chart. Overall, the presented results thus contribute to validating the effectiveness of the long-term vibration-based monitoring system to detect small structural damages in a stage where they are hardly detectable by visual inspections.

The rest of the paper is organized as follows. Section 2 presents the monumental bell-tower and the monitoring system. Section 3 presents the analysis of the response of the bell-tower to the 2016 Central Italy seismic sequence, in terms of (i) recorded accelerations, (ii) effects of the earthquakes on the natural frequencies of vibration and (iii) control

chart produced as output of the SHM system. Section 4 is devoted to interpreting such a response, by assessing post-earthquake structural conditions with the aid of non-linear finite element simulations and, finally, Section 5 concludes the paper.

2. The bell-tower and the long-term SHM system

The case study structure considered in this paper is the 61.4 m high bell-tower of the Basilica of San Pietro located in Perugia, Italy. Erected for the first time in the 13th century, the tower has been significantly modified throughout the centuries, up to its final configuration dating back to the 15th century. Three structural portions can be clearly identified in the tower. These are: (i) the dodecagonal shaft in the first 26 m, made of stone masonry, with large external portions realized in brick masonry as structural rehabilitation measures due to the occurrence of several damages; (ii) the belfry with hexagonal cross section rising up to 40.8 m, architecturally characterized by large Gothic openings and made of brick masonry covered by an external curtain of stone and (iii) the cusp completing the tower on the top, made of brick masonry (see Fig. 1). In 1997, the tower was severely damaged by the Umbria-Marche earthquake (Cattaneo et al, 2000) and it was restored and consolidated in 2001. Damages mostly affected the columns of the belfry and the cusp.

The bell-tower has been continuously monitored since December 9th 2014, through a simple vibration-based SHM system aimed at detecting small damages in the structure that can be caused by low return period earthquakes. The system comprises three high sensitivity (10 V/g) accelerometers, suitable to measure micro tremors induced by traffic and wind, that are installed at the base of the cusp with a configuration that allows to observe both bending and torsional modes (see Fig. 1). Eight temperature and two humidity Tinytag sensors, from Gemini Data Loggers, are also deployed on the structure to better characterize environmental conditions. A sketch of the monitoring system, with indication of the x-y reference system, is shown in Fig. 1.

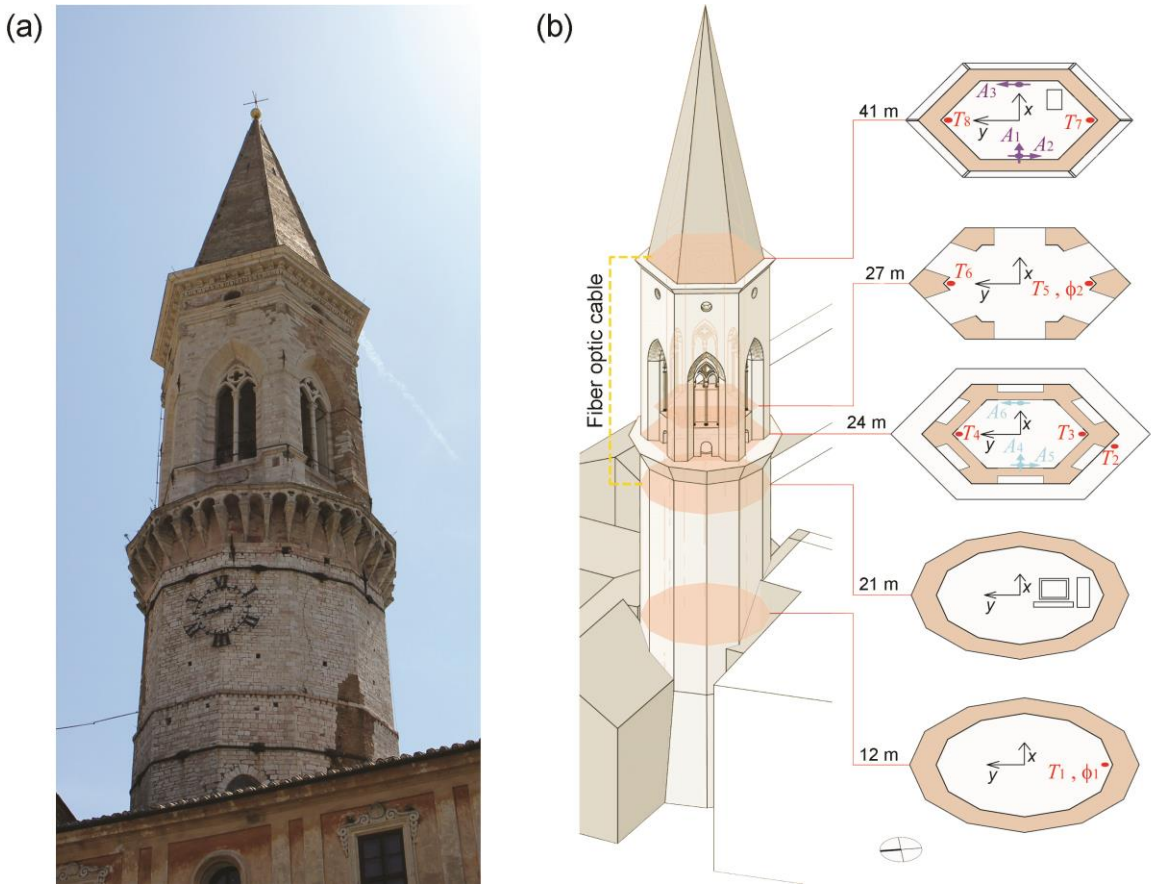

Fig. 1. View of the San Pietro bell-tower (a) and sketch of the structural monitoring system with sensors positions, where A, T and ϕ denote acceleration, temperature and humidity sensors, respectively (b) (A4, A5 and A6 sensors were only used for ambient vibration testing in February 2015, all other sensors are permanently installed on the tower).

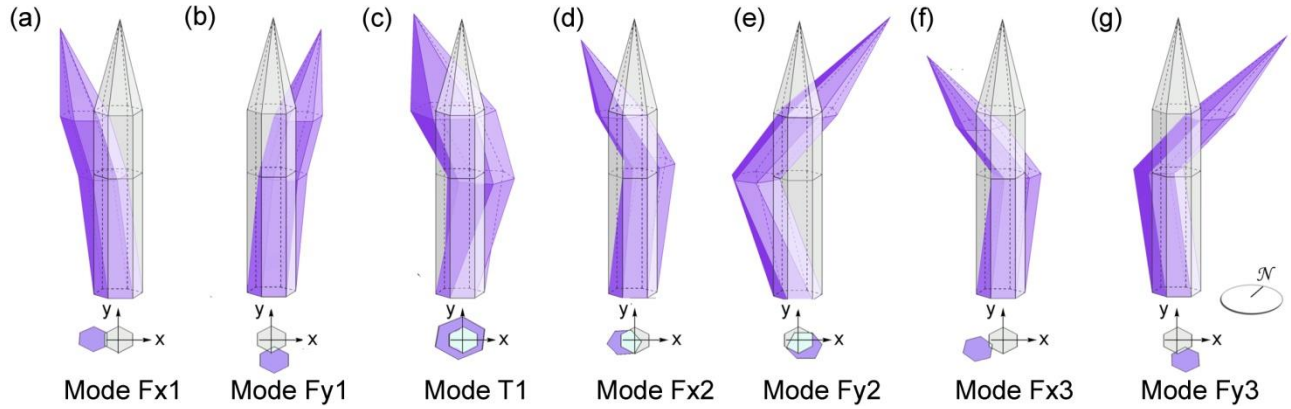

Fig. 2. Identified mode shapes of the bell-tower during the AVT in February 2015.

Table 1. Identified natural frequencies of the bell-tower in the AVT carried out in February 2015 (f_{AVT}) and in the monitoring period (f_{MNT} and $\sigma_{f,MNT}$ denote mean values and standard deviations of identified natural frequencies, respectively, whereby ID success ratio denotes the relative frequency of monitoring data sets in which a natural frequency is consistently identified through SSI) and their reference values at the temperature of 20° C ($f_{20°}$).

Mode no.	Mode type	f_{AVT} [Hz]	f_{MNT} [Hz]	$\sigma_{f,MNT}$ [Hz]	$f_{20°}$ [Hz]	ID success ratio (%)
1	Fx1	1.449	1.468	0.019	1.480	87.82
2	Fy1	1.518	1.533	0.019	1.547	94.31
3	T1	4.342	4.330	0.068	4.294	97.96
4	Fx2	4.575	-	-	4.657	-
5	Fy2	4.889	4.970	0.108	5.044	70.38
6	Fx3	7.245	-	-	7.374	-
7	Fy3	7.263	7.262	0.078	7.255	76.41

Data recorded by the three accelerometers are consecutively stored in files containing 30 minute acceleration time series with a sampling frequency of 100 Hz. A network connection with TCP/IP communication protocol allows to download the data from the computer located on site to a dedicated server placed in the Laboratory of Structural Dynamics of the Department of Civil and Environmental Engineering of University of Perugia. Here, data are processed with the purpose of extracting modal parameters estimates and this information is used for SHM purposes. For the details on automated modal identification, modal tracking and novelty analysis, the interested reader is referred to (Ubertini et al, 2016b).

An ambient vibration test (AVT) was carried out in February 2015, by using six high-sensitivity accelerometers (A1, ..., A6 as shown in Fig. 1 (b)), with the purpose of identifying the main vibration modes of the structure to be tracked by the monitoring system. Seven modes of vibration were identified within the range from 0 to 10 Hz. These modes are three flexural modes in x direction (E-W direction), denoted as Fx1, Fx2, Fx3, three flexural modes in y direction (N-S direction), denoted as Fy1, Fy2 and Fy3, and one torsional mode, T1 (see Fig. 2). Five of these modes, namely Fx1, Fy1, T1, Fy2 and Fy3, have been effectively and consistently identified during the whole monitoring period, while modes Fx2 and Fx3 have not allowed a continuous successful identification and are therefore not useful for monitoring purposes. Tab. 1 summarizes the natural frequencies identified in the AVT, as well as the mean values and the standard deviations of the natural frequencies identified during monitoring, with the associated identification success ratios. Significant variations of identified natural frequencies with changing temperature have been observed in previous work (Ubertini et al, 2017). In this regards, Tab. 1 also reports the natural frequencies of the seven modes after removing temperature effects. This removal has been carried out by means of a Multiple Linear Regression (MLR) of natural frequencies versus temperature, using 20°C as the reference temperature. More specifically, a linear regression model has been established for each natural frequency, using temperature data recorded by the sensor installed in the tower (see Fig. 1) exhibiting the largest statistical correlation coefficient with the same natural frequency. The average correction factor necessary to convert the natural frequencies of bending modes Fx1, Fy1, Fy2 and Fy3 identified in the AVT into their values at the reference temperature of 20°C has been used to also correct the natural frequencies of bending modes Fx2 and Fx3, that have not been consistently identified during the whole monitoring period.

The adopted vibration-based SHM method consists of a MLR model combined with PCA to remove the effects of changes in environmental and operational conditions from time series of natural frequencies and of a control chart based on T^2-statistic to detect deviations from normal conditions possibly related to a structural damage. As the first step of the procedure, tracked modal frequencies are collected in an observation matrix, $\mathbf{Y} \in \mathbb{R}^{n \times N}$, where n is the number of identified frequencies and N is the number of observations. Quantities contained in matrix $\mathbf{Y}$ are affected by changes in environmental conditions and cannot be directly used as damage sensitive features. Quantities contained in a residual error matrix, $\mathbf{E} \in \mathbb{R}^{n \times N}$, are used for this purpose and computed as

$$\mathbf{E} = \mathbf{Y} - \hat{\mathbf{Y}} \tag{1}$$

where $\hat{\mathbf{Y}}$ are modal frequencies independently estimated through a statistical model based on a combination of MLR and PCA. A damage condition is identified as an anomaly in the residuals, under the assumption that damage induces a change in the distribution of $\mathbf{E}$. To this aim, the classic statistical process control tool named *novelty analysis* is adopted, using the T^2-statistic, which is defined as

$$T^2 = r \cdot \left(\bar{\mathbf{E}} - \bar{\bar{\mathbf{E}}}\right)^T \cdot \Sigma^{-1} \cdot \left(\bar{\mathbf{E}} - \bar{\bar{\mathbf{E}}}\right) \tag{2}$$

where $\bar{\mathbf{E}}$ is the mean of the residuals in the subgroup of the last r observations, while $\bar{\bar{\mathbf{E}}}$ and $\mathbf{\Sigma}$ are the mean values and the covariance matrix of the residuals, respectively. Both $\bar{\bar{\mathbf{E}}}$ and $\mathbf{\Sigma}$ are statistically estimated in a reference period in which the structure is supposed to be in the reference healthy state, which is called the *training period*. In the present application, the Upper Control Limit (UCL) of the control chart is statistically computed as the value of T^2 corresponding to a cumulative frequency of 95% in the training period. An anomaly in the data is thus identified in the form of an outlier, that is a value of T^2 greater than the UCL. While there is approximately a 5% probability to observe an outlier when the structure is in the healthy state (false alarm), if a relative frequency of outliers significantly greater than the 5% is steadily observed over time, a change in the statistical distribution of the residuals is supposed to have occurred, so denoting an anomalous structural condition not experienced during the training period. Changes in T^2 are therefore likely to occur after an earthquake producing a damage in a structure. For more details on the adopted mathematical tools for SHM, the interested reader is referred to (Ubertini et al, 2016b).

3. Analysis of monitoring data recorded during the seismic sequence

3.1 The seismic sequence

The 2016 Central Italy seismic sequence, that is under specific investigation in this work, comprised the three following major earthquakes: (i) Accumoli Mw6.0 earthquake occurred on August 24th at 01:36 UTC (epicenter coordinate latitude 42.706° and longitude 13.223°); (ii) Ussita Mw5.9 earthquake occurred on October 26th at 19:18 UTC (epicenter coordinate latitude 42.915° and longitude 13.128°) and (iii) Norcia Mw6.5 earthquake occurred on October 30th at 06:40 UTC (epicenter coordinate latitude 42.84° and longitude 13.11°). Ground motion records for these earthquakes have been obtained from the data provided by the Italian Strong Motion Network (RAN) of the Department of Civil Protection (DPC) and by the Italian Seismic Network (RSN) of the National Institute of Geophysics and Vulcanology (INGV), that manage several accelerometric stations deployed in the Country (Pacor et al, 2011; Gorini et al, 2010).

The San Pietro bell-tower is located at a distance of about 85 km in the NW direction from the epicenter of Accumoli earthquake and approximately 70 km from the epicenters of Ussita and Norcia earthquakes. Fig. 3 shows horizontal acceleration waveforms recorded in Amatrice station, the closest station to Accumoli earthquake's epicenter, during the first major shock and the map of the accelerometric stations between the epicenter and Perugia, with indications of the measured values of the PGA. From the inspection of these data, it is observed that recorded near-field PGA and elastic response amplification are extremely high. Recorded peak accelerations and velocities at several stations along the way from the epicenter towards the bell-tower in Perugia, for each earthquake, are summarized in Tab. 2. The table reports in particular E-W, N-S and vertical components of PGA and PGV (peak ground velocity),

denoted as PGA_E, PGA_N, PGA_Z, PGV_E, PGV_N and PGV_Z, respectively. The table also reports values of PGA_S^R and PGA_S^A, representing estimated values of horizontal PGA on rock site and alluvium site, respectively, according to the Ground Motion Prediction Equation (GMPE) for Italy, a seismic intensity attenuation empirical law calibrated in (Bindi et al, 2009). Recorded ground motion data at the site of the bell-tower are unfortunately not available and the local intensity of the earthquakes needs to be estimated, as discussed in more details in Section 4.

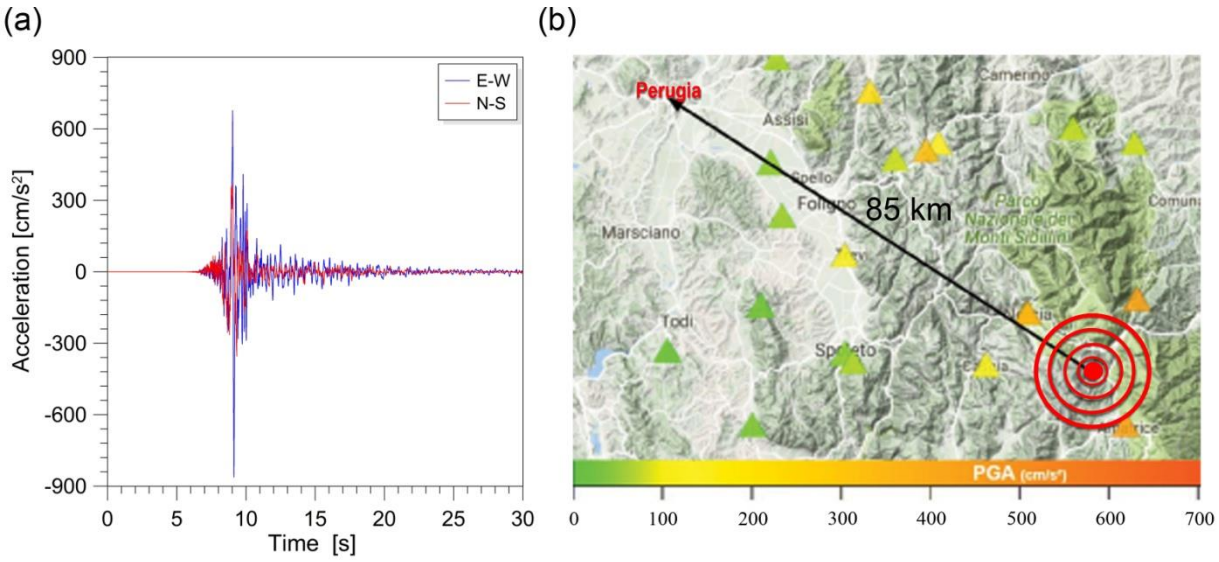

Fig. 3. Accumoli earthquake: E-W and N-S components of near-field acceleration recorded in Amatrice station close to the epicenter (a) and geographical map highlighting PGA values recorded by accelerometric stations, the epicenter of the earthquake and the city of Perugia (b).

Table 2. Synthetic information regarding the three main shocks of 2016 Central Italy seismic sequence (Accumoli Mw6.0 earthquake of August 24th, Ussita Mw5.9 earthquake of October 26th and Norcia Mw6.5 earthquake of October 30th) as recorded by accelerometric stations placed at increasing distances from the epicenters in the direction towards the site of the bell-tower (PGA_E, PGA_N, PGA_Z denote PGA values in E-W, N-S and vertical directions, respectively, PGV_E, PGV_N, PGV_Z are corresponding values of PGV, while PGA_S^R and PGA_S^A are values of horizontal PGA estimated by GMPE empirical attenuation law (Bindi et al, 2009) for rock and alluvium site conditions, respectively).

	Stations	Distance [km]	PGA_E [cm/s^2]	PGA_N [cm/s^2]	PGA_Z [cm/s^2]	PGA_S^R [cm/s^2]	PGA_S^A [cm/s^2]	PGV_E [cm/s^2]	PGV_N [cm/s^2]	PGV_Z [cm/s^2]
Accumoli	Norcia	14.25	331.61	376.96	208.60	139.85	219.12	29.20	19.16	8.74
	Trevi	44.09	71.78	107.58	44.87	47.60	74.57	5.56	7.52	2.57
	Bevagna	56.01	39.78	50.28	36.22	37.56	58.85	5.61	6.92	2.81
	Casteln.-Assisi	61.57	44.34	44.29	17.75	34.19	53.57	7.54	11.70	4.21
	Valfabbrica	71.45	58.81	34.79	14.20	29.49	46.20	1.99	1.78	1.08
	Panicale	94.29	4.02	4.24	2.69	22.37	35.04	0.56	0.51	0.60
	Umbertide	99.65	8.54	9.39	3.44	21.17	33.16	0.75	0.89	0.48
Ussita	Monte Cavallo	13.55	408.58	559.74	529.49	134.51	210.74	11.22	14.32	7.43
	Foligno Seggio	26.20	83.86	106.38	49.53	72.83	114.11	4.80	5.86	2.78
	Fol Prot Civ Reg	35.18	32.45	31.67	26.51	54.67	85.66	58.73	90.06	35.37
	Casteln.-Assisi	45.06	42.86	35.16	12.50	42.85	67.14	105.15	79.77	25.05
	Umbertide	80.37	7.07	8.9	4.23	24.12	37.80	0.68	0.61	0.38
Norcia	Preci	7.93	260.91	315.42	202.52	342.17	536.10	10.89	14.05	6.72
	Foligno	36.26	117.26	86.77	47.84	87.64	137.30	5.66	5.80	3.97
	Casteln.-Assisi	46.33	62.85	65.61	26.84	68.84	107.85	9,71	15.26	5.40

Table 3. Maximum accelerations recorded on top of the bell-tower (corresponding RMS values are reported in brackets) during 2016 Central Italy seismic sequence, under excitation of swinging bells on June 5th 2016, during a wind storm occurred from March 4th to March 6th 2015 and in normal everyday conditions (RMS values only).

	Channel 1 [cm/s^2]	Channel 2 [cm/s^2]	Channel 3 [cm/s^2]	Resultant 1-2 [cm/s^2]
Accumoli	58.61 (9.22)	76.32 (11.09)	79.48 (11.28)	91.40 (14.42)
Ussita	60.65 (8.10)	37.81 (4.91)	30.08 (4.72)	64.45 (9.47)
Norcia	94.23 (15.96)	76.27 (10.18)	64.87 (10.08)	94.69 (18.93)
Bells	3.39 (1.14)	2.78 (0.87)	2.69 (0.84)	3.51 (1.43)
Wind storm	2.49 (0.11)	4.47 (0.09)	2.42 (0.09)	7.19 (0.19)
Normal conditions	(0.02)	(0.02)	(0.02)	(0.02)

Table 4. Maximum velocity obtained by time integration of the accelerations recorded on top of the bell-tower (corresponding RMS values are reported in brackets) during 2016 Central Italy seismic sequence, under excitation of swinging bells on June 5th 2016, during a wind storm occurred from March 4th to March 6th 2015 and in normal everyday conditions (RMS values only).

	Channel 1 [cm/s]	Channel 2 [cm/s]	Channel 3 [cm/s]	Resultant 1-2 [cm/s]
Accumoli	7.17 (1.18)	9.94 (1.35)	10.14 (1.38)	11.26 (1.79)
Ussita	7.25 (1.04)	4.08 (0.57)	3.75 (0.56)	7.69 (1.18)
Norcia	11.97 (2.13)	8.52 (1.22)	7.66 (1.23)	11.97 (2.45)
Bells	0.39 (0.13)	0.31 (0.10)	0.30 (0.09)	0.40 (0.15)
Wind storm	0.23 (0.01)	0.66 (0.01)	0.20 (0.01)	0.66 (0.02)
Normal conditions	(0.002)	(0.002)	(0.002)	(0.002)

3.2 Recorded structural responses during the seismic sequence

Some synthetic information on the response of the bell-tower to the 2016 Central Italy seismic sequence is summarized in Tab. 3, where maximum values and root mean square values of accelerations on top of the tower during the earthquake sequence are reported. Measurement channels are numbered as depicted in Fig. 1(b). In particular, Channel 1 and Channel 2 refer to A1 and A2 sensors, measuring accelerations in *x* (E-W) and *y* (N-S) directions, respectively, while Channel 3 refers to A3 sensor (see Fig. 1(b)) that is deployed in *y* direction. For comparative purposes, Tab. 3 also reports information on the response of the structure under relatively strong dynamic excitations and in normal operational conditions. Two specific cases chosen as representative of relatively strong dynamic excitation are: (i) swinging bells in the morning of June 5th 2016 and (ii) a wind storm of exceptional intensity occurred from March 4th to March 6th 2015. It is noted that earthquake-induced accelerations were at least one order of magnitude greater than those measured in these last two cases and two orders of magnitude greater than those measured in normal everyday conditions. It is also worth noting that Accumoli and Norcia earthquakes determined similar values of the peak structural acceleration, while the peak response to Ussita earthquake was a little smaller. The response of the bell-tower in terms of velocity (estimated by time integration of acceleration records after high-pass filtering), summarized in Tab. 4, yields similar considerations to the response in terms of acceleration, in the sense that it highlights similar values of the maximum structural velocity for Accumoli and Norcia earthquakes and comparatively smaller values for Ussita earthquake.

The time histories of measured accelerations on top of the bell-tower, in *x* (E-W) and *y* (N-S) directions, during the three earthquakes, are shown in Fig. 4. During Accumoli earthquake, acceleration in y direction was predominant with a peak value of 76.31 cm/s^2. On the contrary, during Ussita and Norcia earthquakes, acceleration in x direction was predominant, with peak values of 60.66 cm/s^2 and 94.21 cm/s^2, respectively.

With the aim of evaluating the severity of the earthquakes at the site of the bell-tower, the structural response is compared to the response expected by application of the elastic response spectra prescribed by the Italian technical standard code (NTC08, 2008). In particular, the elastic response spectra associated to return periods of 30, 50 and 475 years have been considered (see Fig. 5) assuming C subsoil category. Fig. 5 shows that earthquake-induced accelerations measured on top of the bell-tower are smaller than accelerations expected by application of the 30 years return period design earthquake. This result allows to comment that, as a consequence of the relatively large distance

from the epicenters, the earthquakes of 2016 Central Italy seismic sequence induced ground accelerations at the site of the bell-tower that can be considered representative of relatively small intensity events, with return periods of the order of some years.

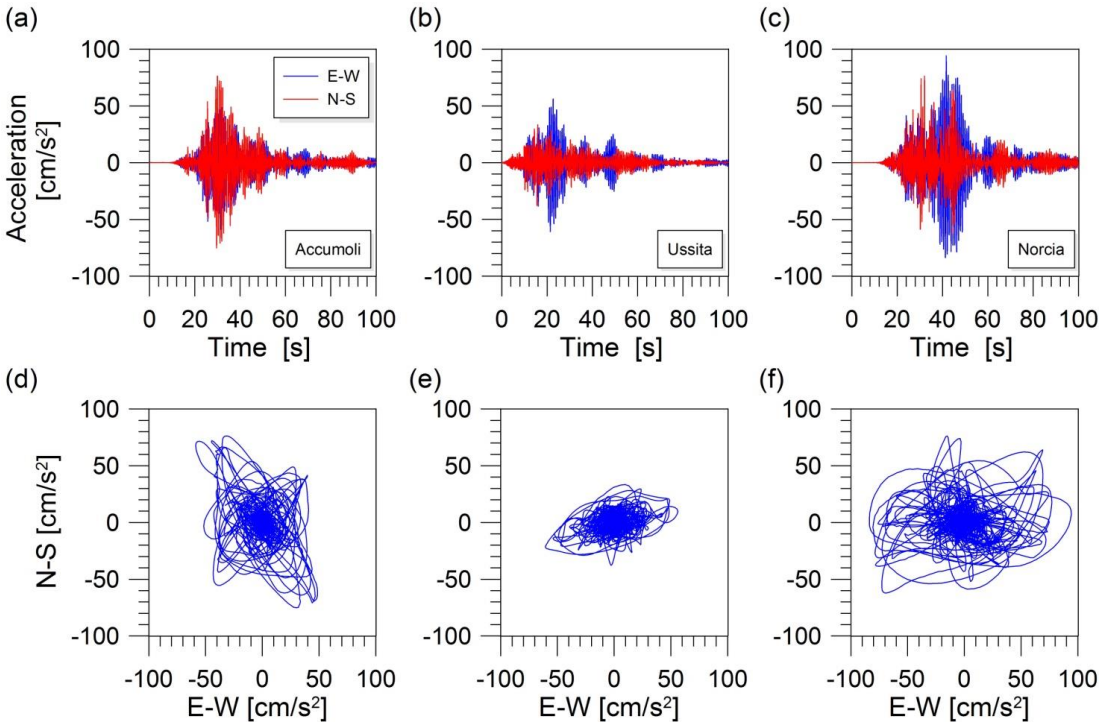

Fig. 4. Measured dynamic response on top of the bell-tower in terms of acceleration during the three main shocks of the seismic sequence: Accumoli earthquake (a,d), Ussita earthquake (b,e) and Norcia earthquake (c,f).

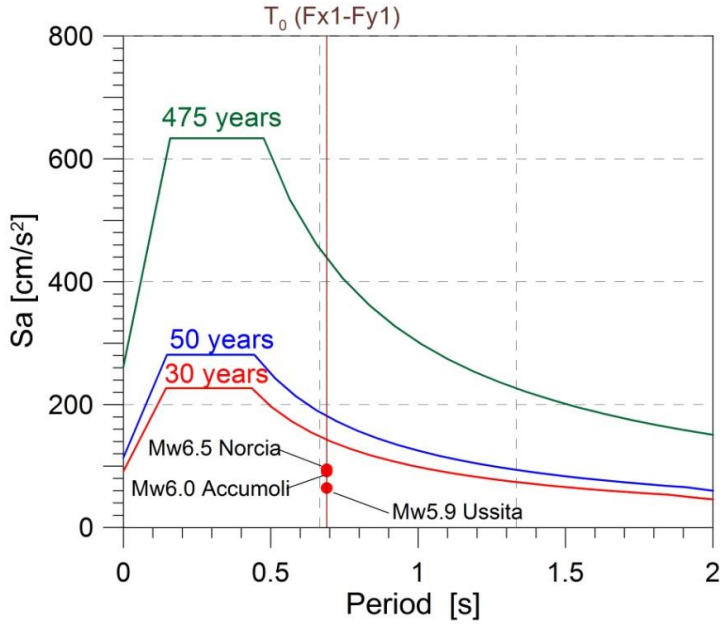

Fig. 5. Elastic response spectra at the site of the bell-tower (Sa denotes the pseudo-acceleration) according to Italian technical standard code (NTC 2008) for different return periods (expressed in years) and comparison with the peak responses recorded on top of the bell-tower during the three main shocks (T_0 denotes the fundamental period of the tower, that is approximately similar for modes Fx1 and Fy1).

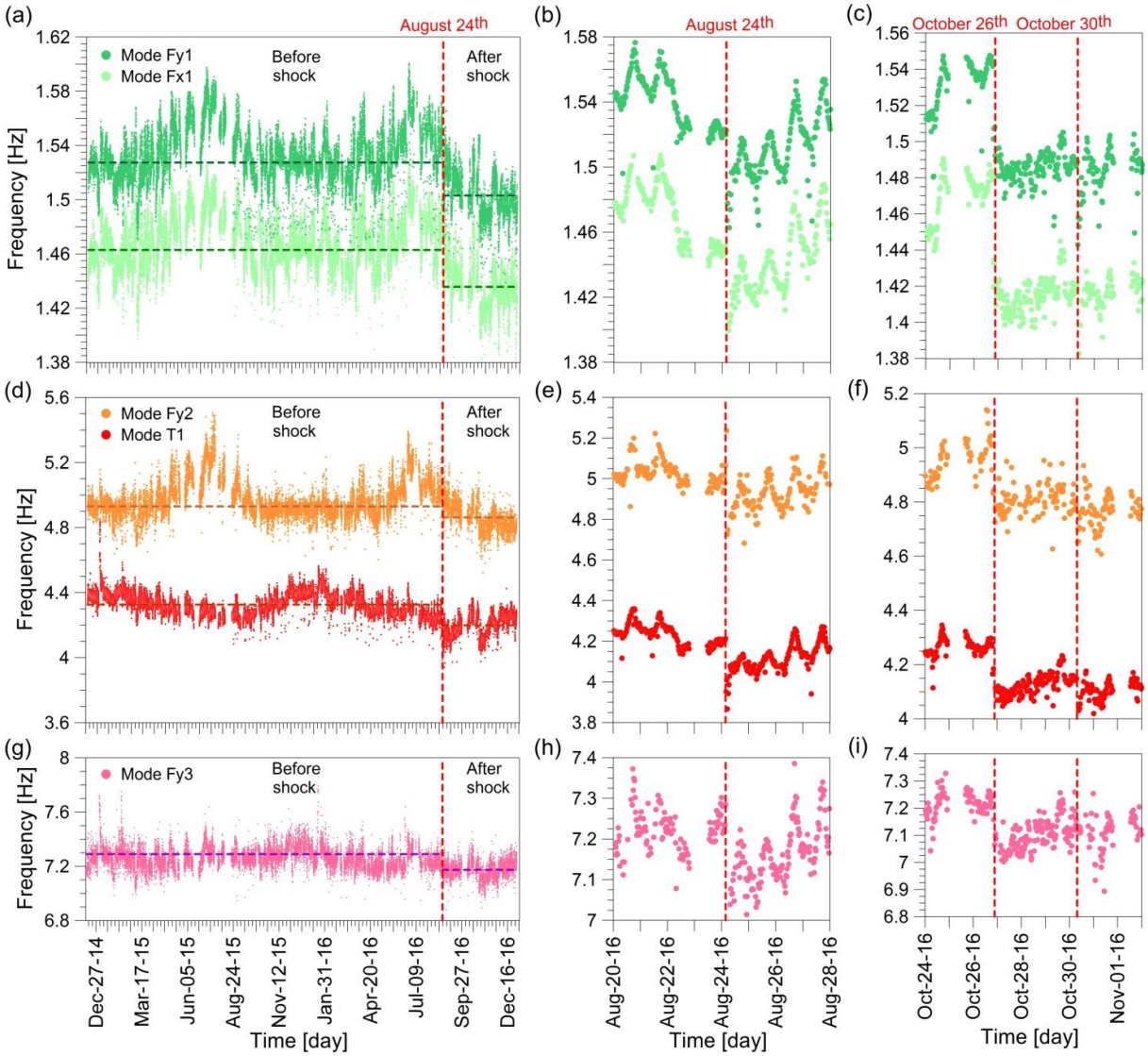

Fig. 6. Time histories of identified natural frequencies of the bell-tower using data of two years of monitoring and detailed views showing earthquake-induced decays immediately after the earthquakes (horizontal dashed lines represent the mean values of the natural frequencies computed in the period from August 24th to December 31st 2016 (after shock) and in the same period of the previous year, 2015 (before shock)): modes Fx1 and Fy1 (a-c); modes Fy2 and T1 (d-f) and mode Fy3 (g-i).

3.3 Permanent earthquake-induced effects on dynamic behavior of the bell-tower

Fig. 6 shows the time histories of the natural frequencies of vibration of the five modes of the bell-tower continuously identified and tracked during the monitoring period (modes Fx1, Fy1, T1, Fy2 and Fy3). Daily and seasonal fluctuations associated to changing environmental conditions and, primarily, ambient temperature, are visible in these plots, as extensively discussed in (Ubertini et al, 2017). More importantly, the plots clearly highlight that permanent frequency decays have occurred during the seismic sequence, whereby the horizontal dashed lines in Figg. 6 (a,d,g) represent the mean values of the natural frequencies computed before and after the first shock. In this regards, in order to have a fair comparison that is not significantly affected by changing environmental conditions, the period from August 24th to December 31st 2016 has been considered to compute the average values of the natural frequencies after the first shock and the same period in the previous year, 2015, has been considered to compute the average values in the reference condition. The vertical dashed lines in all subfigures represent the dates of the three major earthquakes of the seismic sequence, highlighting the instantaneous decays in natural frequencies induced by the same events. In particular, frequency decays are very evident for modes Fx1 and Fy1 in the plots of Fig. 6 (b,c), as well as for mode T1

in the plots of Fig. 6 (e,f). Frequency decays are also apparent, though comparatively less evident, for modes Fy2 (Fig. 6 (e,f)) and Fy3 (Fig. 6 (h,i)).

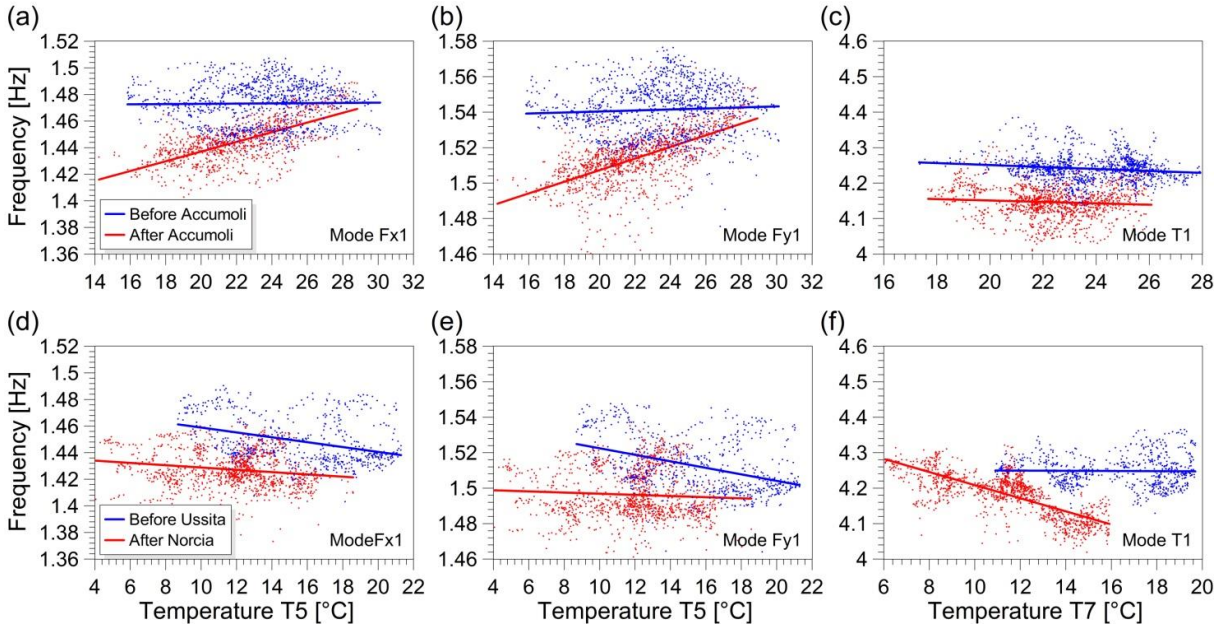

Fig. 7. Identified natural frequencies versus temperature data before and after the main shocks of the seismic sequence and corresponding linear interpolation lines: modes Fx1 (a), Fy1 (b) and T1 (c) 30 days before and 30 days after Accumuli earthquake of August 24th 2016; modes Fx1 (d), Fy1 (e) and T1 (f) 30 days before Ussita earthquake of October 26th 2016 and 30 days after Norcia eartqhuake of October 30th 2016.

In order to investigate in more details and to quantify the decays in natural frequencies caused by the three main earthquake shocks of the seismic sequence, the strong correlation existing between natural frequencies and temperature needs to be taken into account. In this regards, Fig. 7 shows plots of the natural frequencies of the first three vibration modes against measured temperature data, considering 30 days before and 30 days after Accumuli earthquake, as well as 30 days before Ussita earthquake and 30 days after Norcia earthquake. Each natural frequency is plotted against the data recorded by the sensor with which it exhibits the largest statistical correlation coefficient. Consistent earthquake-induced decays in natural frequencies are apparent from these plots, where changes in the slopes of the linear regression lines of frequency versus temperature data are also evidenced. Earthquake-induced frequency decays and their accumulation during the seismic sequence are further investigated in Fig. 8, where natural frequencies identified in time periods of 2015 and 2016 are plotted against temperature data and compared. These results show that frequencies identified in 2015 and 2016 in the period July 24th-August 24th are almost perfectly overlapped. On the contrary, natural frequencies identified in 2016 are clearly shifted downwards with respect to those identified in 2015 after the first shock (period August 25th – September 25th) and further decreased after the second and third shocks (period October 31st – November 30th), what is mostly apparent in the case of the natural frequency of the torsional mode T1. Earthquake-induced relative natural frequency decays are quantitatively evaluated by comparing frequency values identified in the last dataset recorded before each shock, with those identified in the first dataset after each shock. The results are summarized in Tab. 5, where it is shown that Accumoli and Norcia earthquakes induced similar decays in natural frequencies, of the order of 2-3% for modes Fx1 and Fy1, while natural frequency decays caused by Ussita earthquake are relatively smaller. It is also worth noting that torsional mode T1 exhibited the largest frequency decays for both Accumuli and Norcia earthquakes, equal to 6.17% and 3.16%, respectively.

Permanent earthquake-induced effects on the dynamic response of the bell-tower are also highlighted by the control chart generated as output of the vibration-based SHM system. The chart, built according to Eq. (2) by using the time series of identified natural frequencies after removal of the effects of changing environmental conditions according to Eq. (1), is reported in Fig. 9. This chart clearly highlights that a deviation of the structural behavior from normal conditions has occurred after Accumoli earthquake, with a notable increase in the relative frequency of outliers after the shock. Furthermore, as shown in the detailed view of the control chart in the period of the seismic sequence, the effects

of Ussita and Norcia earthquakes are also evident, confirming that the structure has accumulated damage during the seismic sequence.

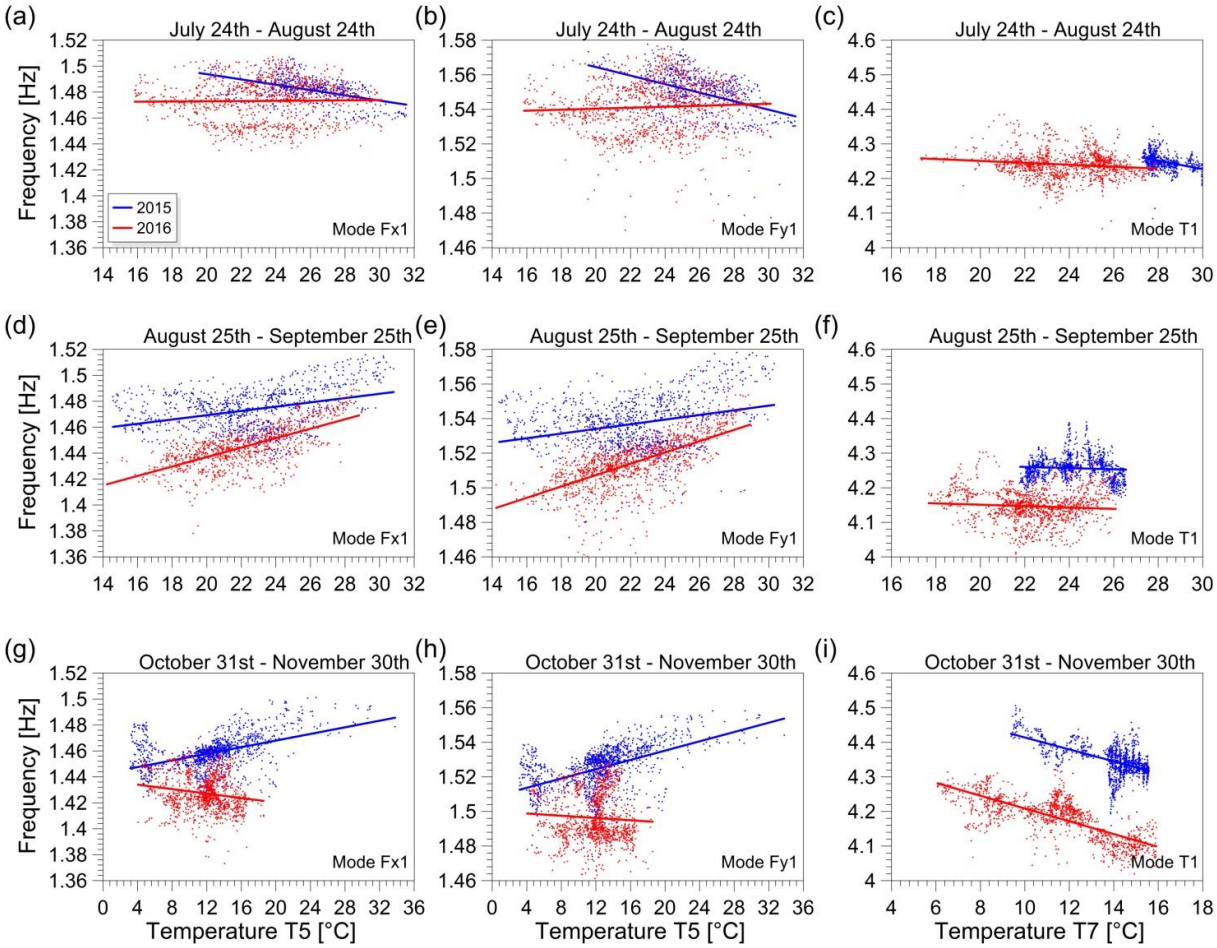

Fig. 8. Comparison of identified natural frequencies versus temperature data in 2015 and 2016 and corresponding linear interpolation lines: mode Fx1 (a), Fy1 (b) and T1 (c) 30 days before August 24th (no earthquake); mode Fx1 (d), Fy1 (e) and T1 (f) 30 days after August 24th (in 2016 data contain the effects of Accumuli earthquake); mode Fx1 (g), Fy1 (h) and T1 (i) 30 days after October 30th (in 2016 data contain the cumulative effects of Accumuli, Ussita and Norcia earthquakes).

Table 5. Relative decays in identified natural frequencies of the bell-tower after the three main shocks of the seismic sequence as obtained from monitoring data.

Earthquake	Frequency decay (%)				
	Fx1	Fy1	T1	Fy2	Fy3
Accumoli	3.79	2.92	6.17	1.30	2.87
Ussita	0.89	0.95	1.48	1.61	0.85
Norcia	2.90	1.87	3.16	2.17	0.26
Cumulated	7.58	5.74	10.81	5.08	3.98

4. Interpretation of monitoring data

4.1 Non-linear numerical model

With the purpose of interpreting monitoring data for structural assessment, the dynamic response of the bell-tower under ground motion has been simulated by a 3D numerical model of the structure, built in the framework of the Finite Element Method (FEM) by using solid hexahedral and tetrahedral elements, with orthotropic constitutive behaviour (see Fig. 10). The numerical model has been calibrated on the basis of the experimentally identified natural modes of vibration by varying the values of uncertain mechanical parameters through an optimization procedure, using

natural frequencies at the reference temperature of 20° C as the target frequencies (see Tab. 1). In order to obtain consistency between numerically and experimentally identified mode shapes, a proper modeling of the restraints given by the neighbouring constructions in the lower part of the bell-tower and, primarily, the basilica and the abbey, was found to be crucial. The main mechanical parameters of the constituent materials, as estimated after model tuning, are summarized in Tab. 6, while target and numerically predicted natural frequencies of vibration of the bell-tower are summarized in Tab. 7. These results highlight an excellent agreement between numerically predicted and experimentally identified natural frequencies, with an average relative deviation, Δf_{mean} between the two quantities lower then 3%. For more details on the model and the calibration procedure, the interested reader is referred to (Ubertini et al, 2016a).

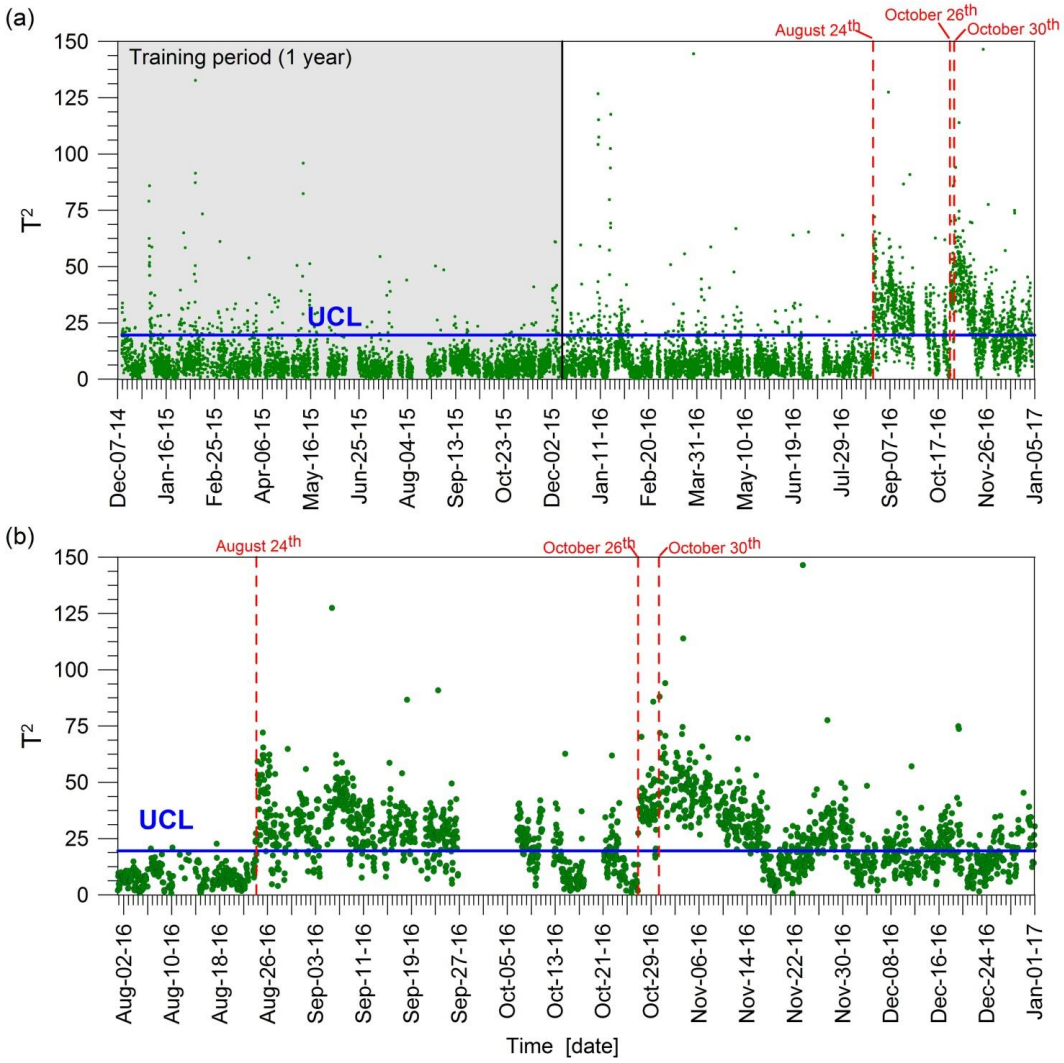

Fig. 9. Control chart of two years of monitoring period (a) and detailed view showing increased number of outliers after the three main shocks of the seismic sequence (b).

Table 6. Parameters assumed in the FE numerical model after calibration.

Structural part	Young's modulus [MPa]	Shear modulus [MPa]	Mass density [t/m^3]	Poisson's ratio [-]
Shaft	4274	1238	2.60	0.25
Belfry	4335	1787	1.75	0.25
Cusp	1800	563	1.89	0.25

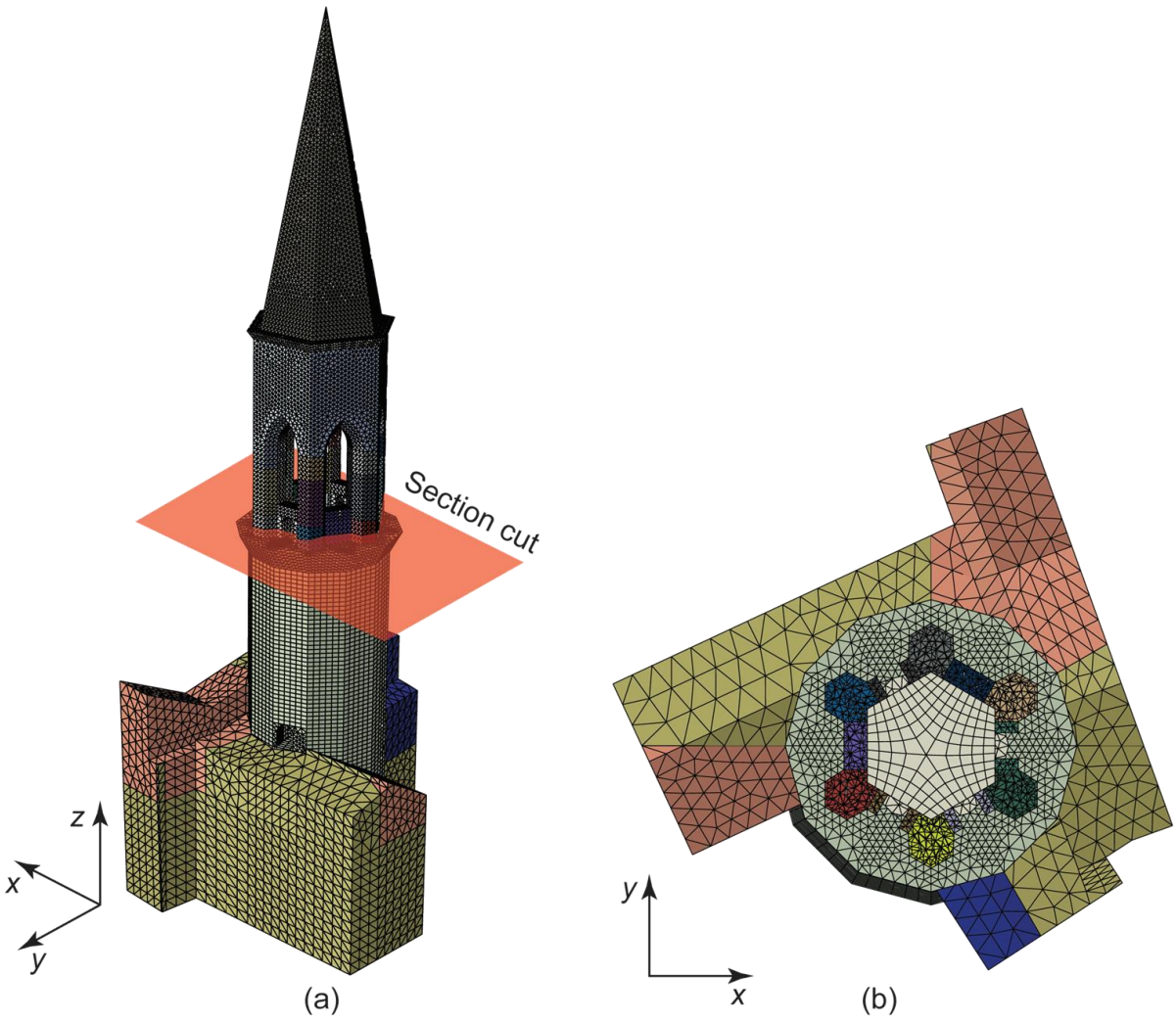

Fig. 10. Sketch of the numerical FE model of the bell-tower: overall view of the computational domain (a) and detailed view of a section cut at the base of the belfry (b).

Table 7. Comparison between experimentally identified natural frequencies at the reference temperature of 20°C ($f_{20°C}$) and numerically predicted ones by FEM analysis (f_{FEM}), where Δf represents the relative difference and Δf_{mean} the mean relative difference.

Mode no.	Mode type	$f_{20°C}$	f_{FEM}	Δf (%)
1	Fx1	1.480	1.439	2.75
2	Fy1	1.547	1.554	0.48
3	T1	4.294	4.294	0.00
4	Fx2	4.657	4.920	5.66
5	Fy2	5.044	5.042	0.03
6	Fx3	7.374	7.172	2.73
7	Fy3	7.255	7.607	4.85
				Δf_{mean}=2.36%

In light of the presented results, the numerical model has been used with some confidence to predict the damage undergone by the structure during the seismic sequence and the associated permanent decays in natural frequencies. In order to reproduce the non-linear mechanical behavior of the masonry, following recent literature works on the seismic vulnerability analysis of masonry towers (Valente and Milani, 2016), the classic concrete damage plasticity model proposed by Lubliner and co-workers (Lubliner et al, 1989) and then modified by Lee and Fenves (Lee

and Fenves, 1998), with tension and compression damage, has been used. Regarding the tension stiffening, the mechanical properties assigned to the materials in different portions of the structure for the description of the failure condition and of the post-peak behaviour as a function of the tensile stresses, σ_t, the cracking strains, $\tilde{\varepsilon}_t^{ck}$, and the damage parameter in tension, d_t (Simulia, 2010), are summarized in Tab.8. It is noted that, in lack of specific experimental test results carried out to evaluate mechanical properties of materials on site, some of the mechanical parameters reported in Tab. 8 have been estimated from the literature, while other parameters have been obtained by means of a manual calibration, by reproducing through numerical simulations the damages caused by the Umbria-Marche earthquake of 1997 and observed during the restoration interventions (Ubertini et al, 2016).

Table 8. Mechanical parameters of tension stiffening and tension damage assumed in the numerical model.

Structural part	σ_t [kN/m^2]	$\tilde{\varepsilon}_t^{ck}$ [-]	d_t [-]
Cusp	220	0.00E+00	0
	140	1.66E-05	0.55
	70	3.86E-04	0.7
	20	5.83E-04	0.9
Belfry	220	0.00E+00	0
	140	7.39E-05	0.45
	70	1.65E-04	0.6
	20	2.44E-04	0.9
Shaft	400	0.00E+00	0
	300	1.75E-04	0.55
	210	3.77E-04	0.8
	40	7.59E-04	0.9

The estimation of damage-induced decays in natural frequencies has been carried out by solving the linear eigenvalue problem of the structure before (undamaged case) and after the non-linear analyses (damaged cases). In particular, in damaged conditions, the following procedure has been adopted. First of all, the weakest parts of the structure, i.e. the structural elements undergoing the largest amounts of damage during the seismic sequence, have been preliminary identified. These weakest structural parts are the pillars of the belfry and the masonry walls comprised between the same pillars at the base of the belfry, some of which are also characterized by openings. Each pillar has been subdivided into three subregions, namely the base, the top and the intermediate region, as shown in Fig. 11. The height of base and top subregions have been assumed equal to column thickness, while the height of the intermediate region corresponded to the remaining portion of each column. Mean values of the tension damage parameter d_t, which is a scalar quantity assuming values in the range 0 ÷ 0.9, where 0 denotes no damage and 0.9 the severely damaged condition, have been estimated in these regions from the results of the non-linear analysis. Finally, the average value of the damage parameter, $\overline{d}_t^{\,i}$, estimated in the *i*th region, has been used to reduce Young, E, and Shear, G, moduli of the material in the same region of the model, according to the following equation:

$$X_d^i = \left(1 - \overline{d}_t^{\,i}\right) X^i \tag{3}$$

with X^i denoting the undamaged value of either E or G in the ith subregion and X_d^i denoting the damaged value of the same quantity.

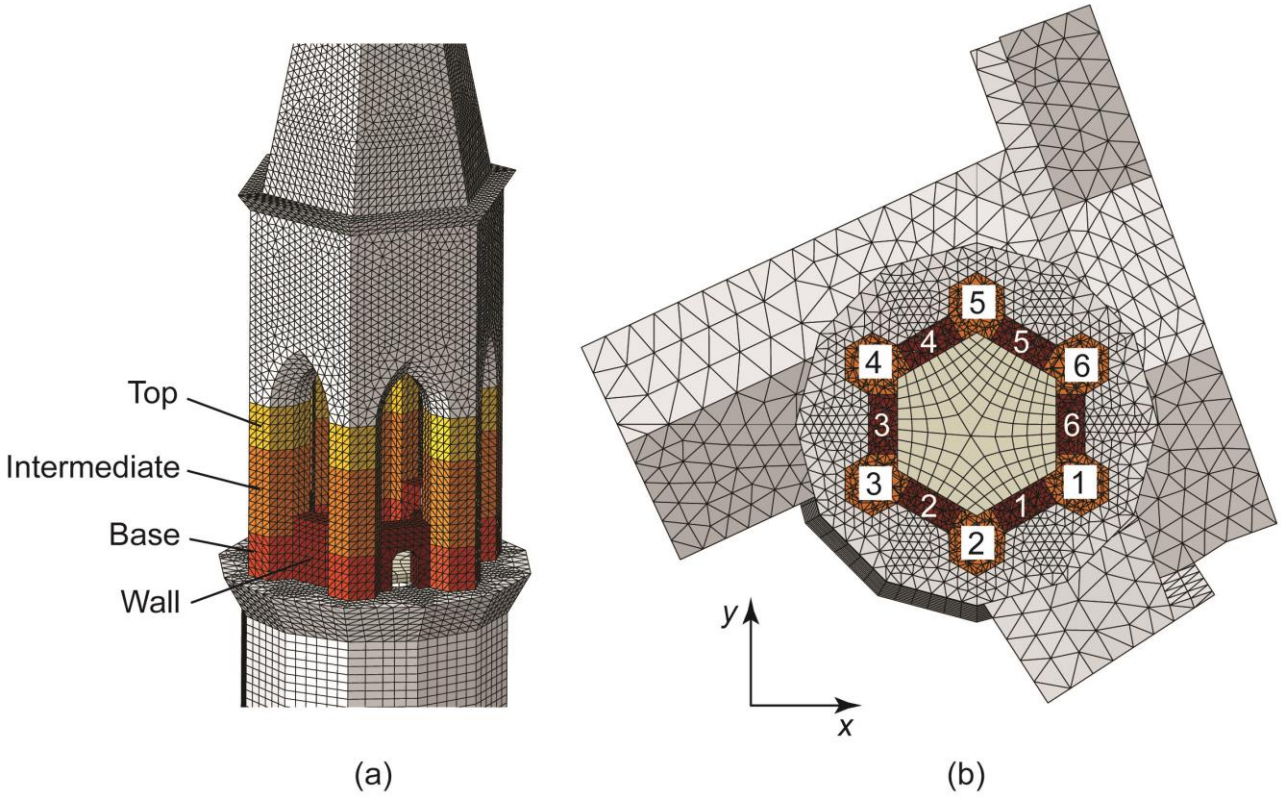

Fig. 11. Detailed view of the computational domain of the numerical model highlighting the structural parts undergoing the largest amount of earthquake-induced damage (top, intermediate and base portions of the columns of the belfry and walls of the belfry) (a) and numbering of columns and walls (b).

4.2 Estimation of far-field seismic inputs

The afore-described non-linear dynamic analysis has required the estimation of the far-field ground motions experienced by the bell-tower during the seismic sequence. As already commented before, due to the relatively large distance between Perugia and the epicenters of the earthquakes, the seismic input at the site of the bell-tower was relatively small. In order to give some more insight on this aspect, Fig. 12 shows the evolution of the ground acceleration all the way along the line from the epicenter to Perugia during Accumoli earthquake, both in terms of waveforms and of elastic response spectra, while Fig. 13 shows PGA values versus epicentral distance. In this last figure, the horizontal PGA values predicted by GMPE model (Bindi et al, 2009) are also reported, assuming both rock and alluvium site conditions.

After an appropriate scaling, the ground motion waveforms of the three main earthquakes of the sequence recorded by the accelerometric station closest to the bell-tower, i.e. Castelnuovo-Assisi (distance from the bell-tower of about 15 km), have been used as inputs for the non-linear FEM analysis. Such ground motion waveforms have been scaled in order to reproduce the expected values of the PGA at the site of the bell-tower, by matching measured and numerically estimated peak acceleration structural responses. More specifically, for each earthquake, the scaling factor has been obtained by a two-step analysis. In a first step, the scaling factor has been estimated as the ratio between measured peak structural acceleration response and the pseudo acceleration obtained by the elastic response spectrum of the ground motion record evaluated at the fundamental natural period of the bell-tower. In a second step, the non-linear response of the bell-tower has been computed using the ground motion record scaled in the previous step. After carrying out this preliminary non-linear dynamic analysis, the scaling factor has been corrected as the ratio between measured and numerically estimated peak acceleration responses. The GMPE approach, accounting for the epicentral distance of the bell-tower, but assuming a homogeneous medium, has been finally considered for comparative purposes, in order to assess if the seismic input estimated by the two-step procedure can be considered as representative of actual conditions. Regarding the vertical direction, for which the GMPE approach is not applicable, the seismic inputs have been scaled using the average scaling factors used for horizontal components.

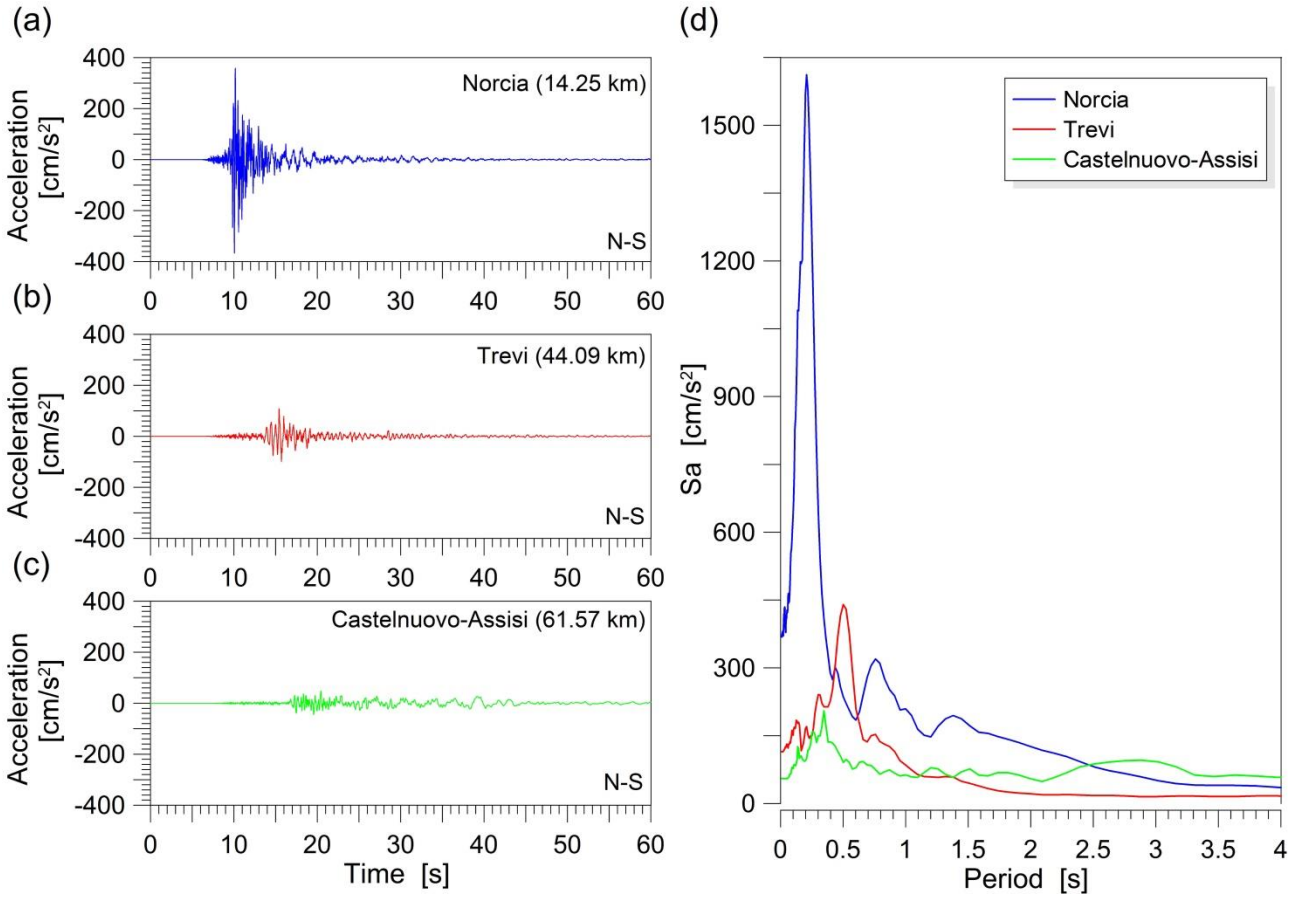

Fig. 12. Evolution of ground acceleration waveforms (N-S components) with epicentral distance for Accumoli earthquake: records of the stations of Norcia (a), Trevi (b) and Castelnuovo-Assisi (c); elastic response spectra of the three acceleration records (d).

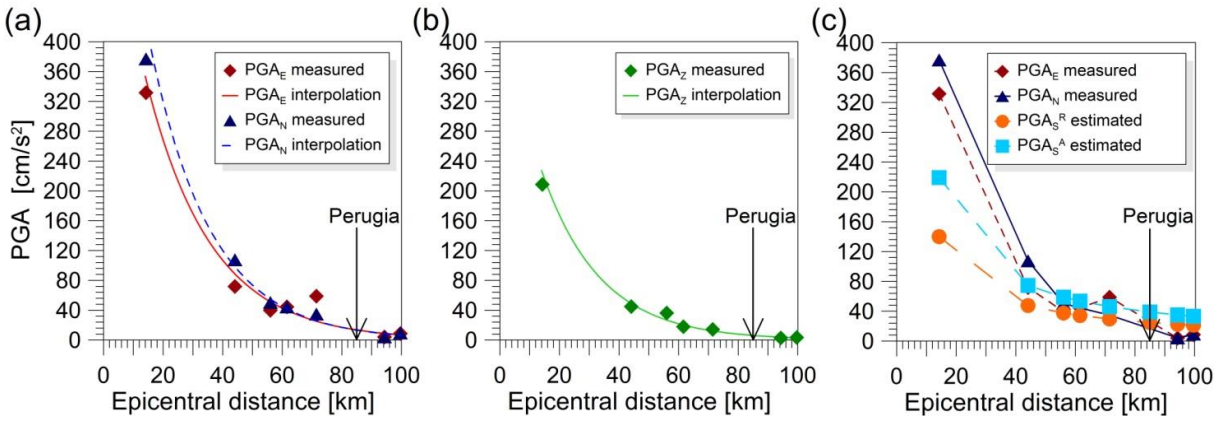

Fig. 13. PGA versus epicentral distance for Accumoli earthquake: values of PGA of E-W (PGA_E) and N-S (PGA_N) components (a) and Z component (b) versus epicentral distance and corresponding exponential interpolation curves; comparison of PGA values measured by accelerometric stations and estimated by GMPE model (Bindi et al, 2009) (c).

The scaling factors used in the numerical analyses and the corresponding far-field PGA values estimated at the site of the bell-tower are summarized in Tab. 9. It is noted that these values are similar to those estimated by GMPE empirical formula, as reported in the same table, though obviously not identical due to the approximations of the same formula. As an example, Fig. 14 shows the time histories of measured and numerically predicted structural accelerations, where the good agreement in terms of peak response accelerations after input scaling is highlighted,

whereby the waveforms are slightly different because, as explained above, the input records to the numerical simulations are unavoidably different from actual ones.

Table 9. Scaling factors applied to the ground motion records of Castelnuovo-Assisi station (15 km far from the bell-tower) in the three main earthquakes of the sequence, corresponding PGA values estimated at the site of the bell-tower and PGA values estimated by application of GMPE prediction model for rock and alluvium medium.

	Accumoli		Ussita		Norcia	
	E	N	E	N	E	N
Scaling factor	0.592	0.696	0.496	0.336	0.664	0.568
Estimated scaled PGA [cm/s^2]	26.25	30.83	21.26	11.81	41.73	37.27
GMPE-rock predicted PGA [cm/s^2]	24.80		27.68		45.19	
GMPE-alluvium predicted PGA [cm/s^2]	38.86		43.37		70.80	

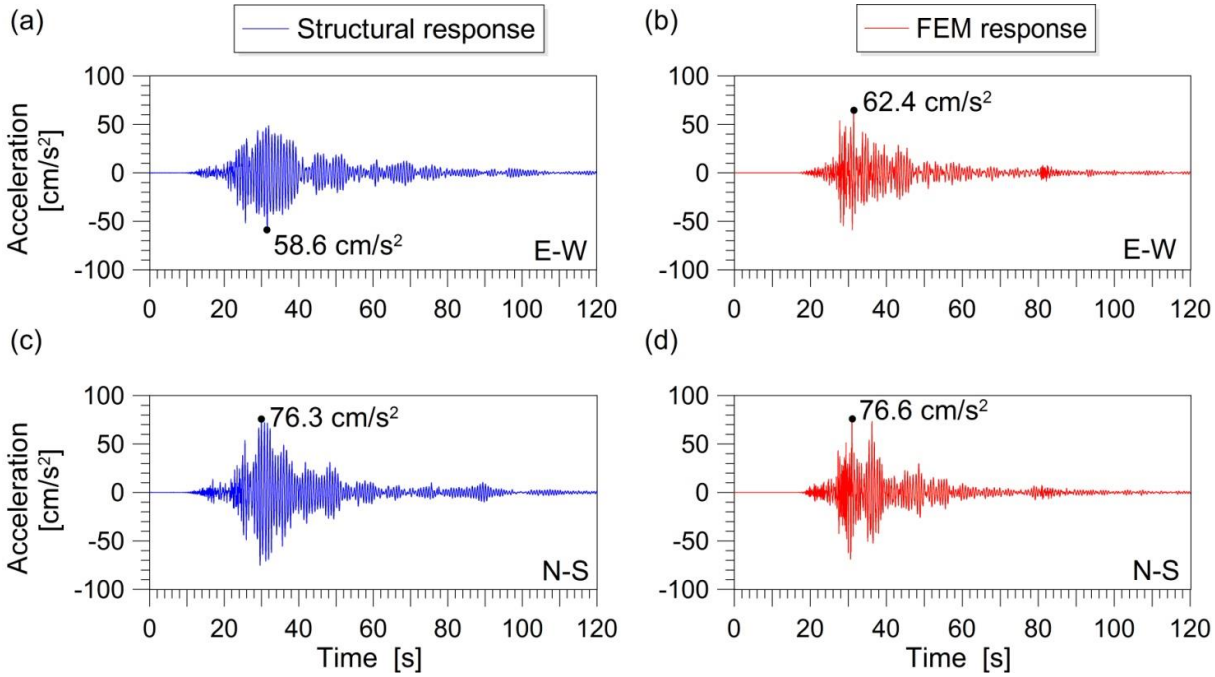

Fig. 14. Comparison between structural response in terms of accelerations measured by accelerometers A1 and A2 (a) and as predicted by FEM simulation using scaled acceleration waveform records of Castelnuovo-Assisi station (see Tab. 9) during Accumoli earthquake.

4.3 Earthquake-induced damage assessment

Nonlinear dynamic analyses using the afore-presented numerical model and scaled seismic inputs have been carried out with the purpose of numerically estimating earthquake-induced structural damages accumulated in the bell-tower during the seismic sequence. In particular, damage accumulation has been considered by concatenating the three scaled waveforms in such a way to carry out a single simulation with sequential application of the three earthquakes.

Fig. 15 shows the maps of the tension damage parameter, d_t, obtained at the end of each seismic input, while the mean values of such a damage parameter, $\overline{d}_t^{\,i}$, in each of the ith damaged structural parts (see Fig. 11) are summarized in Tab. 10. The decays in natural frequencies produced by such earthquake-induced damages have been obtained by carrying out a linear modal analysis before and after reducing the elastic properties of the materials in the damaged regions, according Eq. (3). The results are summarized in Tab. 11 and in Fig. 16 where numerically predicted

decays in natural frequencies are compared to those obtained from field data analysis (see Tab. 5). These results highlight that measured and numerically predicted damage-induced decays in natural frequencies, though obviously not identical, are fully consistent. In particular, they are very similar in terms of their orders of magnitude and the most damage-sensitive modal frequency is consistently the one of the first torsional mode, according to both field data and numerical results. Overall, the average cumulated relative natural frequency decay according to field data analysis is equal to 6.6%, while the same quantity is estimated by numerical finite element analysis as 5.5%.

From the presented considerations, it follows that the deviations from normal conditions of the dynamic behavior of the bell-tower observed after the earthquake shocks in the control chart of Fig. 8 are most likely associated to the formation of microcracks at the base of the columns and in the bottom walls of the belfry of the bell-tower, as well as in the key sections of the pointed arches of the same belfry. As verified by the authors, such damages are hardly detectable by a simple visual inspection and, in any case, difficulty distinguishable from the physiological microcracking of a masonry structure. Overall, the results presented in the paper thus represent a contribution to demonstrating the effectiveness of long-term vibration-based SHM in the realm of earthquake engineering.

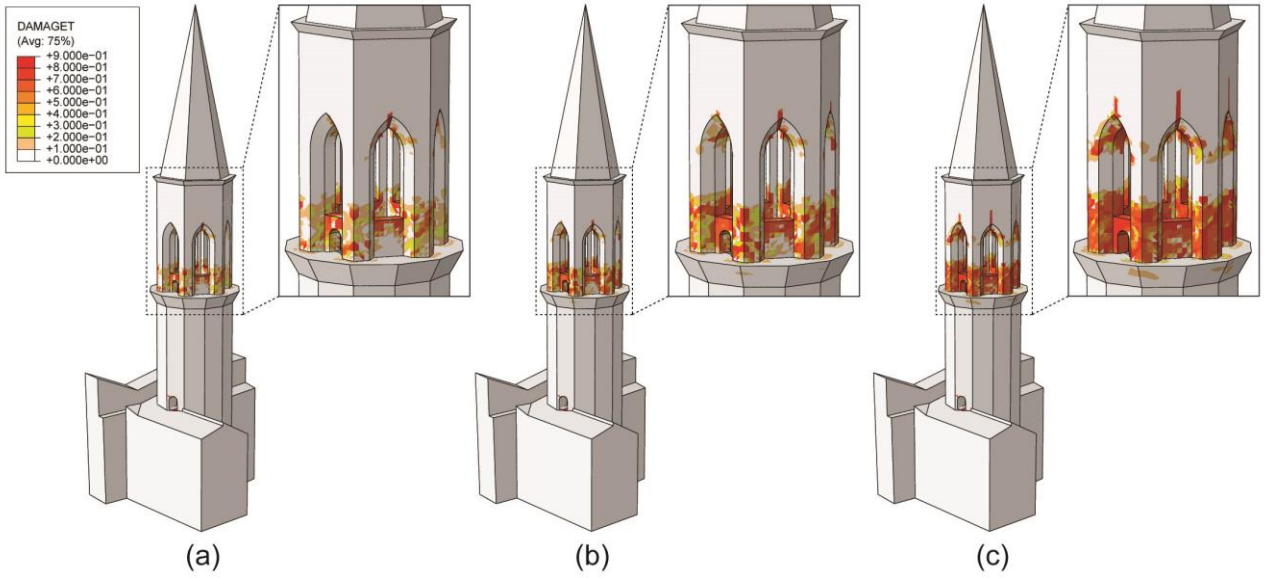

Fig. 14. Maps of tension damage predicted by numerical simulation after the sequential application of Accumoli (a), Ussita (b) and Norcia earthquakes (c).

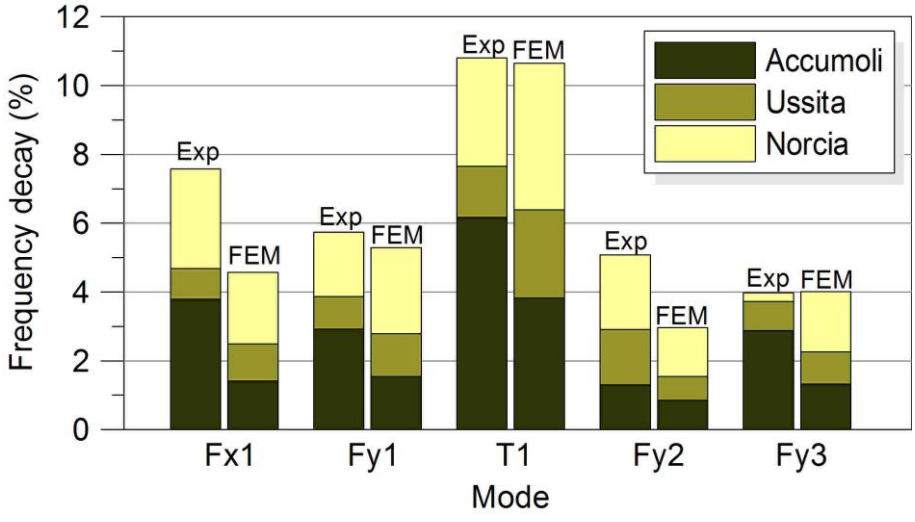

Fig. 15. Comparison between experimentally (Exp) and numerically (FEM) evaluated relative natural frequency decays after Accumoli, Ussita and Norcia earthquakes.

Table 10. Numerically computed mean damage parameters in different portions (identification number #id) of the pillars (P) and of the bottom walls (W) of the belfry, computed by non-linear analysis under sequential application of the three earthquake inputs (B, I and T denote base, intermediate and top portions of each pillar).

#id	Accumoli				Ussita				Norcia			
P/W	$\bar{d}_t^B$	$\bar{d}_t^I$	$\bar{d}_t^T$	$\bar{d}_t^W$	$\bar{d}_t^B$	$\bar{d}_t^I$	$\bar{d}_t^T$	$\bar{d}_t^W$	$\bar{d}_t^B$	$\bar{d}_t^I$	$\bar{d}_t^T$	$\bar{d}_t^W$
1	0.129	0.053	0.007	0.362	0.245	0.107	0.009	0.550	0.405	0.217	0.024	0.664
2	0.142	0.058	0.008	0.386	0.259	0.135	0.019	0.525	0.418	0.270	0.056	0.649
3	0.116	0.111	0.012	0.241	0.230	0.161	0.015	0.324	0.397	0.289	0.041	0.481
4	0.122	0.073	0.007	0.408	0.204	0.127	0.010	0.579	0.353	0.256	0.032	0.664
5	0.105	0.068	0.007	0.226	0.176	0.163	0.017	0.302	0.351	0.305	0.053	0.423
6	0.100	0.100	0.008	0.405	0.187	0.156	0.010	0.548	0.355	0.276	0.029	0.652

Table 11. Comparison between experimentally (Exp) and numerically (FEM) evaluated relative natural frequency decays after Accumoli, Ussita and Norcia earthquakes.

Earthquake	Frequency decay (%)											
	Fx1		Fy1		T1		Fy2		Fy3		Average	
	Exp	FEM	Exp	FEM	Exp	FEM	Exp	FEM	Exp	FEM	Exp	FEM
Accumoli	3.79	1.41	2.92	1.54	6.17	3.83	1.30	0.85	2.87	1.32	3.54	1.91
Ussita	0.89	1.08	0.95	1.24	1.48	2.56	1.61	0.69	0.85	0.94	1.23	1.39
Norcia	2.90	2.09	1.87	2.50	3.16	4.27	2.17	1.41	0.26	1.75	2.52	2.57
Accumulated	7.58	4.58	5.74	5.29	10.81	10.65	5.08	2.96	3.98	4.01	6.64	5.50

5. Conclusions

The paper has presented analysis and interpretation of the response of a continuously monitored monumental masonry bell-tower located in Perugia, Italy, to the 2016 Central Italy seismic sequence. The tower is a notable scientific benchmark that has been the object of previous studies by the authors, including more than two years of long-term vibration-based monitoring, application of automated modal identification and multivariate statistical analysis techniques for damage detection, finite element modeling and non-linear seismic analysis. The long-term SHM system is based on the use of a control chart that automatically reveals deviations of the structural behavior from normal conditions, possibly associated to a small structural damage, by using information from the time series of five continuously identified natural frequencies of vibration of the structure, after removal of environmental and operational effects through principal component analysis and multivariate linear regression.

The tower is located at a distance of about 85 km in the NW direction from the epicenter of Accumoli Mw6.0 earthquake (August 24th 2016, 01:36 UTC) and at similar distances from the epicenters of the two other major shocks of the seismic sequence, namely Ussita Mw5.9 earthquake (October 26th 2016, 19:18 UTC) and Norcia Mw6.5 earthquake (October 30th 2016, 06:40 UTC). Nevertheless, all the three earthquakes were able to produce a significant structural response, whose analysis gives the opportunity to better evaluating the role of long-term vibration-based SHM in the context of earthquake engineering and preventive conservation of historic structures. The following are the main results achieved within the paper.

(i) The recorded accelerations on top of the tower during the three main earthquake shocks highlighted similar peak values, approximately equal to 1 m/s^2. As discussed in the paper, this kind of response can be considered as representative or relatively low intensity earthquakes at the site of the bell-tower, whose return period can be estimated in the order of some years. Nevertheless, the output control chart of the SHM system highlighted permanent deviations of the structural behavior from normal conditions occurred after all earthquakes, with a notable increase in the number of outliers right after the first shock.

(ii) The warning generated by the control chart suggested to carry out a visual inspection of the structure. Unfortunately, the extent of existing small cracks in the structure was not known a priori, which does not allow any quantitative comparison of the two scenarios before and after the earthquakes. However, no relevant damage was observed past the seismic sequence in any part of the structure that could be clearly distinguished from the physiological microcracking of a masonry structure.

(iii) The results of the control chart also suggested to closely inspect the time series of the natural frequencies of the structure which revealed that, right after the earthquake shocks, all natural frequencies exhibited consistent decays. In the case, for instance, of the first shock, these frequency decays were about equal to 3.8% and 2.9% for the first two bending modes, 6.2% for the torsional mode and about 1.3% and 2.9% for two higher order bending modes. Similar decays in natural frequencies were also observed after the two other earthquakes, with the natural frequency of the torsional mode systematically exhibiting the largest decays. Decays in natural frequencies were also confirmed by comparing plots of natural frequencies versus measured temperatures, using data recorded in 2015 and in 2016.

(iv) The origin of the previously highlighted frequency decays was investigated by non-linear finite element analysis using a model of the structure optimally calibrated on the basis of monitoring data. Far-field PGA values at the site of the tower were estimated by seeking for a good match between recorded and computed accelerations on top of the tower, in this way calibrating the inputs for the finite element simulation, taking predictions from a classic seismic intensity empirical attenuation law as references. The finite element simulation highlighted that the columns and the base walls of the belfry are the weakest parts of the structure, undergoing the formation of micro-cracks under tensile stresses during the three main earthquake shocks of the seismic sequence.

(v) Earthquake-induced decays in natural frequencies were estimated by a linear modal analysis carried out through the finite element model in the damaged configurations, after the sequential application of the three seismic inputs. The results showed that the observed frequency decays are fully consistent with the numerically predicted ones. Experimental and numerical results were also in good agreement in regards to the largest damage sensitivity of the natural frequency of the first torsional mode. These results allow to conclude, with a certain level of confidence, that the observed deviations of the structural behavior from normal conditions have been caused by small damages induced by the three earthquakes, consisting of microcracks at the base of the columns of the belfry, as well as in some key sections of the pointed arches in the same structural portion. While such damages are not necessarily associated to a reduction in safety and in the vertical load bearing capacity of the structure, they still represent a permanent modification in the structural behavior, whose possible evolution has to be monitored in the future.

Overall, the present paper has demonstrated that long-term vibration-based SHM systems based on continuous automated modal identification in a changing environment can reveal the formation of earthquake-induced damages in heritage structures at a stage where such damages are not detectable by a mere visual inspection. This is especially important during seismic sequences, when there is the need to promptly install adequate safety provisions on the most vulnerable structures to avoid possible collapses, in the general framework of preventive conservation of heritage structures exposed to the seismic hazard.

Acknowledgements

This project has received funding from the European Union's Framework Programme for Research and Innovation HORIZON 2020 under grant agreement No 700395.

References

Aras F, Krstevska L, Altay G, Tashkov L (2011) Experimental and numerical modal analyses of a historical masonry palace. Constr Build Mater 25:81–91.

Bellino A, Fasana A, Garibaldi L, Marchesiello S (2010) PCA-based detection of damage in time-varying systems. Mech Syst Signal Proc 24:2250–2260.

Benedettini F, De Sortis A, Milana G (2017) In field data to correctly characterize the seismic response of buildings and bridges. Bulletin of Earthquake Engineering 15(2):643–666.

Bennati S, Nardini L, Salvatore W (2005) Dynamic behaviour of a medieval masonry bell tower. II. Measurement and modelling of the tower motion. J Struct Eng 131:1656–1664.

Bindi D, Luzi L, Pacor F, Sabetta F, Massa M (2009) Towards a new reference ground motion prediction equation for Italy: update of the Sabetta--Pugliese (1996). Bulletin of Earthquake Engineering 7(3):591–608.

Bindi D, Iervolino I, Parolai S (2016) On-site structure-specific real-time risk assessment: perspectives from the REAKT project. Bulletin of Earthquake Engineering 14(9):2471–2493.

Bodeux J, Golinval JC (2001) Application of ARMAV models to the identification and damage detection of mechanical and civil engineering structures. Smart Mat Struc 10(3):479.

Brencich A, Sabia D (2008) Experimental identification of a multi-span masonry bridge: the Tanaro Bridge. Constr Build Mater 22:2087–2099.

Casarin F, Modena C (2008) Seismic Assessment of Complex Historical Buildings: Application to Reggio Emilia Cathedral, Italy. Int J Archit Herit 2(3):304–327.

Cattaneo M, Augliera P, De Luca G, Gorini A, Govoni A, Marcucci S, Michelini A, Monachesi G, Spallarossa D, Trojani L, Xgums (2000) The 1997 Umbria-Marche (Italy) earthquake sequence: analysis of the data recorded by the local and temporary networks. Journal of Seismology 4(4):401–414.

Comanducci G, Ubertini F, Materazzi A (2015) Structural health monitoring of suspension bridges with features affected by changing wind speed. JWind Eng Ind Aerodyn 141:12–26.

Comanducci G, Magalhes F, Ubertini F, Cunha (2016) On vibration-based damage detection by multivariate statistical techniques: Application to a long-span arch bridge. Structural Health Monitoring 15(5):505–524,

Cross E, Worden K, Chen Q (2011) Cointegration: a novel approach for the removal of environmental trends in structural health monitoring data. Proceedings of the Royal Society of London A: Mathematical, Physical and Engineering Sciences 467(2133):2717–2732.

Cross E, Koo K, Brownjohn J,Worden K (2013) Long-term monitoring and data analysis of the Tamar Bridge. Mech Syst Signal Pr 35(1-2):16 – 34.

Cross EJ, Worden K (2012) Cointegration and why it works for SHM. Journal of Physics: Conference Series 382(1):012,046.

Cury A, Cremona C (2012) Assignment of structural behaviours in long-term monitoring: Application to a strengthened railway bridge. Structural Health Monitoring 11(4):422–441.

Deraemaeker A, E R, De Roeck G, Kullaa J (2008) Vibration-based structural health monitoring using output-only measurements under changing environment. Mech Syst Signal Proc 22(1):34 – 56.

Dervilis N, Choi M, Taylor S, Barthorpe R, Park G, Farrar C, Worden K (2014) On damage diagnosis for a wind turbine blade using pattern recognition. Journal of Sound and Vibration 333(6):1833 – 1850.

Dervilis N,Worden K, Cross E (2015) On robust regression analysis as a means of exploring environmental and operational conditions for SHM data. Journal of Sound and Vibration 347:279 – 296.

Ditommaso R, Mucciarelli M, Parolai S, Picozzi M (2012) Monitoring the structural dynamic response of a masonry tower: comparing classical and time-frequency analyses. Bulletin of Earthquake Engineering 10(4):1221–1235.

Dolce M, Nicoletti M, De Sortis A, Marchesini S, Spina D, Talanas F (2017) Osservatorio sismico delle strutture: the Italian structural seismic monitoring network. Bulletin of Earthquake Engineering 15(2):621–641.

Farrar CR, Beck JL (2015) Special Issue of Earthquake Engineering and Structural Dynamics on earthquake engineering applications of structural health monitoring. Earthquake Engineering Structural Dynamics 44(4):499–500.

Farrar CR, Worden K (2012) Structural Health Monitoring: A Machine Learning Perspective. John Wiley & Sons, Ltd.

Foti D, Diaferio M, Giannoccaro N, Mongelli M (2012) Ambient vibration testing, dynamic identification and model updating of a historic tower. NDT & E Int 47:88–95.

Fugate ML, Sohn H, Farrar CR (2001) Vibration-based damage detection using statistical process control. Mechanical Systems and Signal Processing 15(4):707 – 721.

Fuller WA (2009) Introduction to statistical time series, vol 428. John Wiley & Sons.

Gentile C, Gallino N (2008) Ambient vibration testing and structural evaluation of a historic suspension footbridge. Adv Eng Softw 39:356–366.

Gentile C, Saisi A (2007) Ambient vibration testing of historic masonry towers for structural identification and damage assessment. Constr Build Mater 21:1311–1321.

Gentile C, Saisi A (2013) Operational modal testing of historic structures at different levels of excitation. Constr Build Mater 48:1273–1285.

Gentile C, Saisi A, Cabboi A (2015) Structural Identification of a Masonry Tower Based on Operational Modal Analysis. Int J Archit Herit 9(2):98–110.

Gorini A, Nicoletti M, Marsan P, Bianconi R, De Nardis R, Filippi L, Marcucci S, Palma F, Zambonelli E (2010) The Italian strong motion network. Bulletin of Earthquake Engineering, 8(5):1075–1090.

Goulet J, Michel C, Kiureghian AD (2015) Data-driven post-earthquake rapid structural safety assessment. Earthquake Engineering Structural Dynamics 44(4):549–562.

Ivorra S, Pallars FJ (2006) Dynamic investigations on a masonry bell tower. Eng Struct 28(5):660 – 667.

Jaishi B, Ren W, Zong Z, Maskey P (2003) Dynamic and seismic performance of old multitiered temples in Nepal. Eng Struct 25:1829–1839.

Kambhatla N, Leen TK (1997) Dimension reduction by local principal component analysis. Neural Computation 9(7):1493–1516.

Kaya Y, Safak E (2015) Real-time analysis and interpretation of continuous data from structural health monitoring (SHM) systems. Bulletin of Earthquake Engineering 13(3):917–934.

Lee J, Fenves G (1989) Plastic-Damage Model for Cyclic Loading of Concrete Structures. Journal of Engineering Mechanics 124:892–900.

Lubliner J, Oliver J, Oller S, O˜nate E (1989) A Plastic-Damage Model for Concrete. International Journal of Solids and Structures 25(3):229–326.

Magalhes F, Cunha A, Caetano E (2009) Online automatic identification of the modal parameters of a long span arch bridge. Mech Syst Signal Proc 23(2):316 – 329.

Magalhes F, Cunha A, Caetano E (2012) Vibration based structural health monitoring of an arch bridge: From automated OMA to damage detection. Mech Syst Signal Proc 28:212–228.

Mosavi A, Dickey D, Seracino R, Rizkalla S (2012) Identifying damage locations under ambient vibrations utilizing vector autoregressive models and Mahalanobis distances. Mech Syst Signal Proc 26:254 – 267.

NTC08 (2008) Norme Tecniche per le Costruzioni (in Italian). Italian Ministry of Infrastructures and Transport.

Ntotsios E, Papadimitriou C, Panetsos P, Karaiskos G, Perros K, Perdikaris PC (2008) Bridge health monitoring system based on vibration measurements. Bulletin of Earthquake Engineering 7(2):469

Oh CK, Sohn H (2009) Damage diagnosis under environmental and operational variations using unsupervised support vector machine. Journal of Sound and Vibration 325(1-2):224–239.

Pacor F, Paolucci R, Luzi L, Sabetta F, Spinelli A, Gorini A, Nicoletti M, Marcucci S, Filippi L, Dolce M (2011) Overview of the Italian strong motion database ITACA 1.0. Bulletin of Earthquake Engineering 9(6):1723–1739.

Pea F, Loureno PB, Mendes N, Oliveira DV (2010) Numerical models for the seismic assessment of an old masonry tower. Eng Struct 32(5):1466 – 1478.

Peeters B, De Roeck G (2001) One-year monitoring of the Z 24-Bridge: environmental effects versus damage events. Earthquake Eng Struct 30(2):149–171.

Pitilakis K, Karapetrou S, Bindi D, Manakou M, Petrovic B, Roumelioti Z, Boxberger T, Parolai S (2016) Structural monitoring and earthquake early warning systems for the AHEPA hospital in Thessaloniki. Bulletin of Earthquake Engineering 14(9):2543–2563.

Ponzo FC, Ditommaso R, Auletta G, Mossucca A (2010) A fast method for structural health monitoring of Italian reinforced concrete strategic buildings. Bulletin of Earthquake Engineering 8(6):1421–1434.

Rainieri C, Fabbrocino G (2010) Automated output-only dynamic identification of civil engineering structures. Mech Syst Signal Proc 24(3):678 – 695.

Ramos L, Marques L, Loureno P, DeRoeck G, Campos-Costa A, Roque J (2010) Monitoring historical masonry structures with operational modal analysis: two case studies. Mech Syst Signal Proc 24:1291–1305.

Ramos L, Aguilar R, Loureno P (2011) Operational modal analysis of historical constructions using commercial wireless platforms. Struct Health Monit 10:511–521.

Reynders E, Houbrechts J, Roeck GD (2012) Fully automated (operational) modal analysis. Mechanical Systems and Signal Processing 29:228 – 250.

Saisi A, Gentile C, Guidobaldi M (2015) Post-earthquake continuous dynamic monitoring of the Gabbia Tower in Mantua, Italy. Constr Build Mater 81:101 – 112.

Simulia (2010) Abaqus Analysis User's Manual. Volume III: Materials. Dessault Syst`emes, USA.

Sohn H,Worden K, Farrar CR (2002) Statistical Damage Classification Under Changing Environmental and Operational Conditions. Journal of Intelligent Materials Systems and Structures, 13(9):561–574.

Spina D, Lamonaca BG, Nicoletti M, Dolce M (2011) Structural monitoring by the Italian Department of Civil Protection and the case of 2009 Abruzzo seismic sequence. Bulletin of Earthquake Engineering 9(1):325–346.

Ubertini F, Gentile C, Materazzi A (2013) Automated modal identification in operational conditions and its application to bridges. Eng Struct 46:264–278.

Ubertini F, Cavalagli N, Comanducci G, Materazzi A, Pisello A, Cotana F (2016a) Automated post-earthquake damage detection in a monumental bell tower by continuous dynamic monitoring. In: Structural Analysis of Historical Constructions: Anamnesis, diagnosis, therapy, controls - Proceedings of the 10th International Conference on Structural Analysis of Historical Constructions, SAHC 2016, pp 812–819.

Ubertini F, Comanducci G, Cavalagli N (2016b) Vibration-based structural health monitoring of a historic bell-tower using output-only measurements and multivariate statistical analysis. Structural Health Monitoring 15(4):438–457.

Ubertini F, Comanducci G, Cavalagli N, Pisello AL, Materazzi AL, Cotana F (2017) Environmental effects on natural frequencies of the San Pietro bell tower in Perugia, Italy, and their removal for structural performance assessment. Mechanical Systems and Signal Processing 82:307 – 322.

Valente M, Milani G (2016) Seismic assessment of historical masonry towers by means of simplified approaches and standard (FEM). Construction and Building Materials 108:74 – 104.

Vidal F, Navarro M, Aranda C, Enomoto T (2014) Changes in dynamic characteristics of Lorca RC buildings from pre- and post-earthquake ambient vibration data. Bulletin of Earthquake Engineering 12(5):2095–2110.

Worden K, Manson G, Fieller N (2000) Damage detection using outlier analysis. J Sound Vibr 229(3):647–667.

Worden K, Sohn H, Farrar C (2002) Novelty detection in a changing environment: regression and interpolation approaches. J Sound Vib 258(4):741 – 761.

Yan A, Kerschen G, De Boe P, Golinval J (2005a) Structural damage diagnosis under varying environmental conditions part I: a linear analysis. Mech Syst Signal Proc 19(4):847 – 864.

Yan A, Kerschen G, De Boe P, Golinval J (2005b) Structural damage diagnosis under varying environmental conditions part II: local pca for non-linear cases. Mech Syst Signal Proc 19(4):865 – 880.

Yong L, Feng G (2005) A novel time-domain auto-regressive model for structural damage diagnosis. J Sound Vibr 283(3):1031–1049.